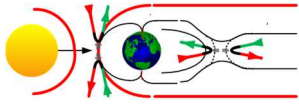


# Observations of Ultralow Frequency Waves at Anchorage, Alaska

Whitham D. Reeve

## Introduction



The solar wind is the agent for many interesting geomagnetic phenomena recorded by ground magnetometers. Among these are Ultralow Frequency Waves (*ULF Waves*), the modern name given to periodic variations in Earth's magnetic field observed on the ground. The phenomenon has been known throughout the years by several other names including *micropulsations* and *magnetic pulsations*. ULF waves have frequencies of a few mHz to a few Hz, corresponding to periods from several minutes to fractions of a second.

Not long after installing a SAM-III magnetometer at Anchorage in 2009, I noticed what I called at the time *noisy periods* on the magnetograms (figure 1). These noisy periods seemed to follow times when coronal hole high-speed streams (CHHSS) became geoeffective or when transient magnetic events were recorded. More than a decade later, after an inquiry in fall 2021 to geomagnetic expert Dr. Michael Hartinger [Reeve21], I finally came to realize that these events were ULF Waves. My initial search for technical information using the keyword *micropulsations* only yielded scientific papers from the 1950s and 1960s because I did not realize that the terminology had changed to ULF Waves after the early 1960s. Online searches using the keywords *ULF Waves* resulted in many up-to-date papers.

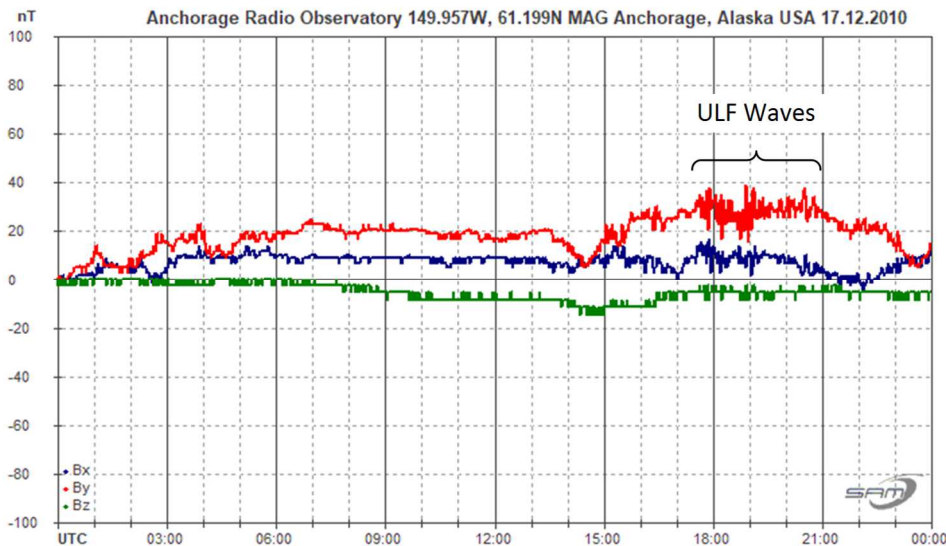


Figure 1 ~ ULF waves possibly instigated by multiple CHHSS on 17 December 2010. The magnetic field traces initially show some relatively smooth and typical variations for a quiet magnetic day. However, at about 1730 UTC, the field experienced short-period pulsations with peak-to-peak amplitudes up to about 20 nT. More detailed analysis, described later, indicates the presence of several frequencies.

I started studying ULF Waves because of curiosity and soon learned of their importance to the science of the magnetosphere. ULF Waves have wavelengths comparable to the scale size of the magnetosphere and play a fundamental role in transporting energy throughout the geospace system. Scientific investigations of ULF Waves reveal information about the magnetosphere's particle density and structure, particularly in the parts of the magnetosphere that are hard to directly measure. An ultimate goal of these studies is a better understanding of space weather and its effects on people and technology. In spite of considerable work over many years, the

causes of ULF Waves are not yet fully understood. Indeed, the scientific literature contains conflicts in many details.

This paper contains two parts: Part I provides 1) a tutorial on ULF Waves, 2) ULF Wave classifications, 3) a brief description of the Anchorage Radio Observatory, and 4) a description of the SAM-III magnetometer used to collect the data; Part II provides descriptions of ULF Wave observations at Anchorage, Alaska from 2010 to 2022 and a discussion of those observations.

---

### Part I-1. ULF Waves

ULF Waves are generated in the magnetosphere, which is the region of space that is dominated by Earth's magnetic field. The magnetosphere has many features (figure 2). Electrons and ions are charged particles (plasma) that exist everywhere in the magnetosphere and have a continuous and wide range of energies. The movement, or drift, of these particles constitute electric currents. Widely separated regions of the magnetosphere are interconnected, or coupled, by these currents. The most familiar currents are the equatorial ring currents, auroral electrojets and magnetic field aligned currents but other current systems exist. The magnetosphere has more than just magnetic fields, it also has electric fields associated with the plasma. The magnetosphere contains several regimes that overlap to some extent but are distinguishable by the types of particles and their energies.

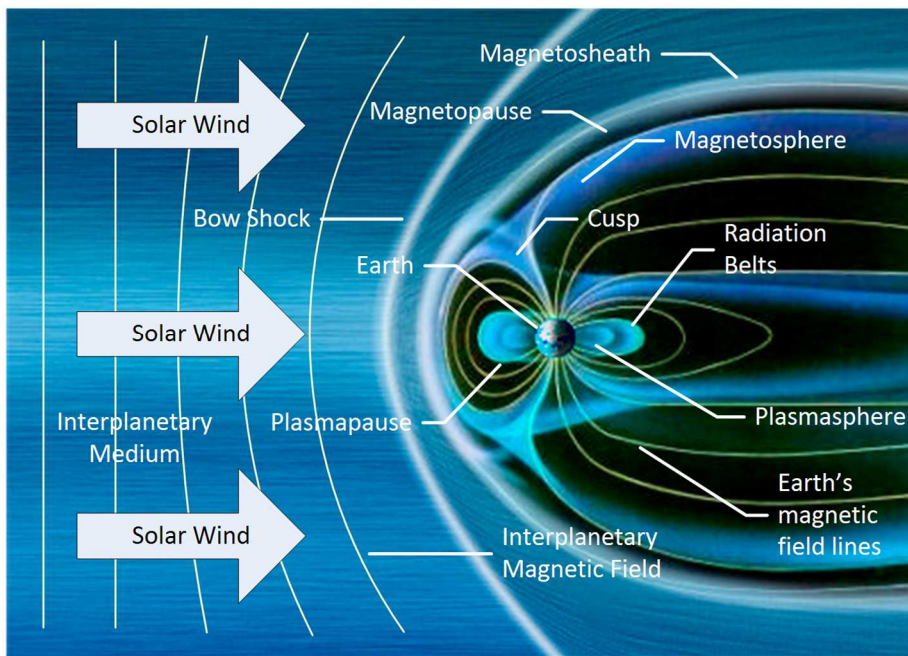


Figure 2 ~ Two-dimensional slice of Earth's magnetosphere and surrounding components that are important in the generation of ULF Waves. The bow shock at the upstream outer edge of Earth's magnetosphere is where the solar wind starts to interact with Earth's magnetic field. The magnetosheath is a turbulent region in which charged particle flows are heavily influenced by the solar wind plasma. The magnetopause is the boundary where Earth's magnetic field is balanced by the IMF and inside which Earth's magnetic field dominates. The plasmasphere starts just above the ionosphere. Underlying image source: [ESA](#)

The magnetosphere is highly distorted and heavily influenced by the solar wind. The solar wind consists of a flow of charged particles from the Sun, mostly hydrogen and helium ions and electrons, and an embedded magnetic field called the *interplanetary magnetic field*, or IMF. The solar wind compresses the magnetosphere on the dayside to about 6 to 10 Earth radii and stretches it out on the nightside to possibly 1000 Earth radii.

On a large scale, the solar wind flows around the magnetosphere cavity when the IMF is primarily northward with respect to Earth's field; however, if the IMF has a southward component, opposite Earth's northward magnetic field, the IMF and Earth's field can merge. The merging of the IMF with Earth's dayside field allows the solar wind plasma to enter the magnetosphere. The merged field lines are open on the dayside and they move to the magnetotail where they close by reconnection on the nightside. This interaction can produce aurora, geomagnetic storms and other phenomena.

The interaction of the solar wind and IMF with the magnetosphere also produces two holes at the high latitude regions facing the Sun, one in each hemisphere. These *polar cusps* (also called auroral cusps) are fixed in space with respect to the Sun as the Earth rotates below. They are characterized by open magnetic field lines that allow charged particles in the solar wind to enter the magnetosphere, transferring mass, momentum, and energy as they mix and collide with Earth's atmosphere. This makes the cusps a source of intense ULF Waves of all frequency ranges.

Within the magnetosphere is the *plasmasphere*, another region that plays an important role in ULF Wave generation. The plasmasphere overlaps the ionosphere and extends above it to 3 or 4 Earth radii (Earth's radius is approximately 6370 km). It is a region of dense, cold (low energy) plasma that surrounds the Earth – a donut within a donut – and rotates with it. Although plasma is found everywhere in the magnetosphere, the plasmasphere usually contains the coldest plasma (least energetic charged particles). The plasmapause is where the plasma density rapidly decreases. The plasmasphere constantly changes. It contracts under quiet solar conditions because of the lower rate of ionization and expands under active solar conditions because of the higher rate of ionization.

The magnetosphere has a natural state of equilibrium that is disturbed by abrupt solar wind pressure and density variations and merging of Earth's magnetic field with the IMF. Perturbations by even small pressure pulses compress or inflate the magnetosphere and excite it into different oscillation modes generally categorized as *Field line resonances*; *Waveguide and cavity modes*; and *Kelvin-Helmholtz Waves* (figure 3). The magnetospheric cavity has natural frequencies of oscillation based on the electric and magnetic conditions. The resulting wave interactions and resonances within the magnetospheric quasi-spherical cavity and waveguide produce ULF Waves with a variety of frequencies and spectral structure. ULF Waves also transport energy from place to place in the magnetosphere; for example, energy initially stored in the magnetotail is thought to be transported by ULF Waves toward Earth and couple to auroral emissions.

Field line resonances: Field line resonances are waves along magnetic field lines that have several modes including harmonics. The different modes are called *toroidal* or *poloidal* depending on how the magnetic field line is excited (figure 4). Toroidal modes are oscillations in azimuth of the magnetic field while poloidal modes are oscillations in the radial direction with respect to Earth. The mode depends on how the solar wind perturbations were coupled through the magnetosphere to excite the field lines.

Cavity modes: The ionosphere is a conducting medium that forms the inner boundary of the cavity and controls the formation and properties of the standing field line resonances. The outer boundary is thought to be the bow shock or magnetopause. The magnetospheric cavity is considered to be similar to a bell in which resonances occur at only certain frequencies depending on material (plasma density and magnetic field strength), geometry

(magnetosphere shape and latitude) and dimensions (figure 5). It is thought that Periodic Density Structures (PDS) in the solar wind directly affect or are the driver of the ULF Wave frequencies in the cavity.

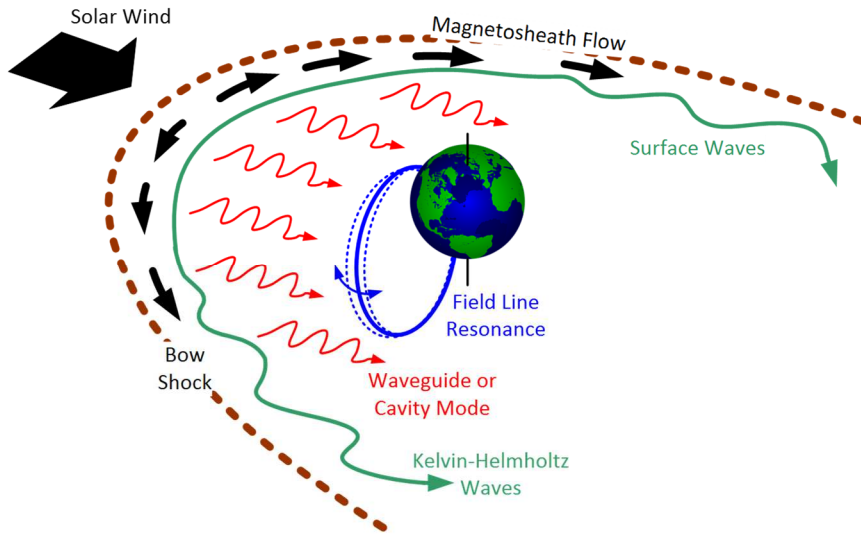


Figure 3 ~ Responses of the magnetosphere to solar wind variations. Three types are shown: 1) Field Line resonance (blue), the movement of magnetic field lines and roughly analogous to the twang of a stretched rubber band or the strings on a guitar; 2) Waveguide or cavity mode (red) produced in the spherical waveguide and analogous to a woodwind instrument such as a flute; and 3) Kelvin-Helmholtz Waves (green) due to shear and turbulence as the solar wind flows over the magnetosphere and analogous to wind over lake or ocean water. Illustration adopted from [Rea].

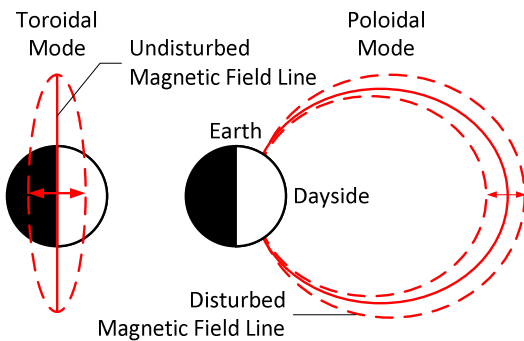


Figure 4 ~ Two-dimensional conceptual illustration of field line resonance modes. Left: Toroidal mode. A view along the plane of a magnetic field line, shown as a solid line, with the field line in Earth's dawn or dusk sector. In the toroidal mode the field line is perturbed in azimuth as shown by the dashed lines. Right: Poloidal mode. A view facing at a right angle to the plane of a magnetic field line, shown as a solid line. The field line is on Earth's dayside. In the poloidal mode, the field line is perturbed in a radial direction as shown by the dashed lines. Image adopted from [Hughes]

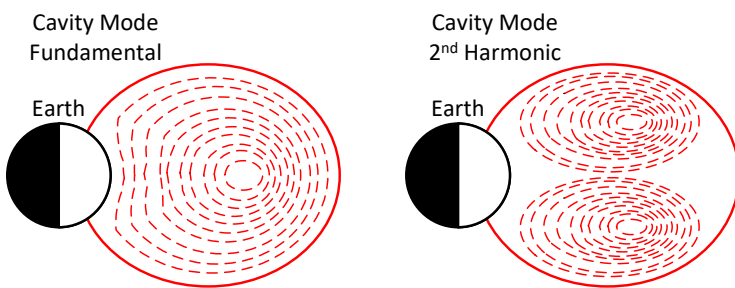


Figure 5 ~ Two-dimensional conceptual illustration of cavity modes. A magnetic field line extends from the dayside of Earth where pressure variations in the solar wind excite the cavity, producing oscillations shown as dashed lines. Earth's ionosphere is the Earth-side boundary of the cavity at the foot of the magnetic field line. Left: Fundamental. Right: 2<sup>nd</sup> Harmonic. Image adopted from [Yumoto]

Resonances appear when the frequency of a stimulus matches the natural frequencies, called *eigenfrequencies*, of the cavity. In the case of the magnetosphere, the stimulus is a pressure pulse in the solar wind, periodic pressure pulses, or possibly sporadic magnetic reconnections. Any of these could provide a broadband energy source to the magnetosphere and resolve to the natural frequencies of the cavity. The cavity's natural frequencies efficiently transport the energy at just those frequencies to magnetic field lines in the magnetosphere. The field lines with natural frequencies that match one of the cavity natural frequencies then resonate strongly.

Kelvin-Helmholtz Waves: The magnetosphere and solar wind act in many ways like two fluids of charged particles in magnetic fields and can be studied as hydromagnetic (or magnetohydrodynamic, MHD) systems. Instabilities occur when there is velocity shear in a fluid, such as in the magnetosphere, or a velocity difference between two fluids such as the solar wind and magnetosphere. These instabilities produce waves or swirls (figure 6) and are called *Kelvin-Helmholtz Waves* (KHW) or Kelvin-Helmholtz Instabilities (KHI). A familiar and visible example of KHW is the waves produced by terrestrial wind (one fluid) blowing over a lake or ocean (another fluid) or the formation of some cloud types in Earth's or Jupiter's atmosphere.

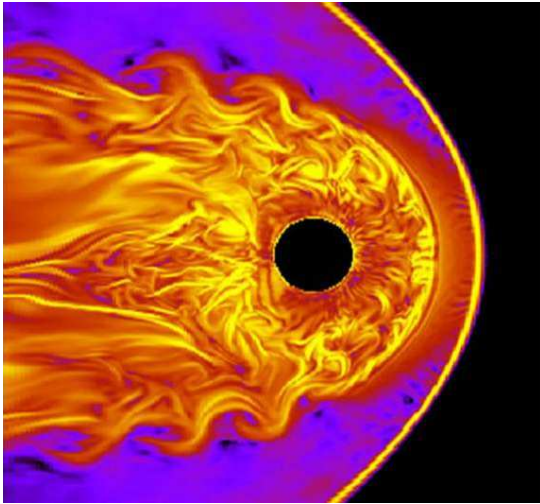


Figure 6 ~ Solar wind flow over the magnetosphere produces swirls called Kelvin-Helmholtz waves or Kelvin-Helmholtz instabilities illustrated by the simulation shown here. Kelvin-Helmholtz Waves are thought to be important for plasma entry and excitation of ULF waves, which in turn strongly affect the radiation belts. The Sun is out of the image to the right and the solar wind flow is right-to-left. The bow shock is the bright curved line on the right and Earth is the black circle. Solar wind plasma enters Earth's magnetosphere through magnetic reconnection when the IMF has a strong and persistent southward component. However, when the IMF is northward, reconnection at the magnetosphere's dayside is unlikely. Image source: NASA-GSFC

The observed characteristics of ULF Waves by ground magnetometers depend on many factors including geographic location, particularly latitude, whether the magnetometer station is on the dayside or nightside of Earth, and the ground conductivity beneath the magnetometer location. Thus, measurements of ULF Waves taken at one location may differ from measurements taken at the same time at another location. Historically, ULF Waves were first unknowingly observed as rapid changes in the current polarity on telegraph wires. Formal observations in the 1850s used a microscope at the end of a very long compass needle to study the pulsations and they were called at the time *micropulsations*. Ground magnetometers, spacecraft and spacecraft clusters and terrestrial HF radars currently are used to study ULF Waves.

ULF Waves observed on the ground must propagate through the ionosphere where they are affected by the ionosphere's properties. In turn, the fields of the propagating ULF Waves can affect the ionosphere's electron density and distribution and, thus, affect the total electron content (TEC) of the ionosphere and radio propagation through it. In this way, ULF Waves in the mHz range can affect the propagation of signals at much higher frequencies. For example, the accuracies of position, navigation and timing (PNT) signals of Global Navigation Satellite Systems (GNSS), such as the Global Positioning System (GPS), are well-known to be affected by the TEC. Radio astronomy observations are affected in a similar way.

ULF Waves often appear with magnetic bays either afterwards or superposed on the bay itself with the appearance of modulating the bay (figure 7). A bay is a magnetic disturbance whose trace on a magnetogram resembles an indentation in a coastline lasting a few hours. The bay may be seen as an increase or decrease in the measured field. A bay indicates the main phase of a geomagnetic storm or substorms and correlates well

with the appearance of visible aurora. When the bay has a high gradient, aurora radio reflections at HF have been observed at Anchorage [Reeve22A]. Bays are discussed in more detail later.

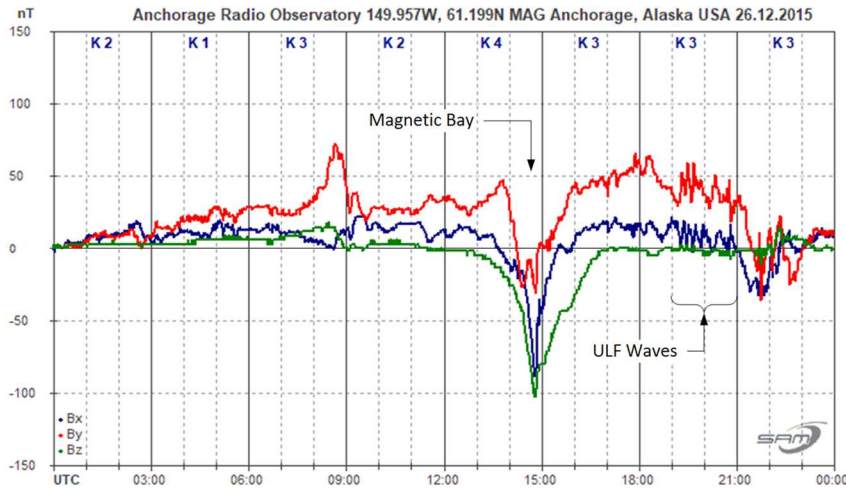


Figure 7.a ~ Magnetic bay beginning about 1300 and recovering 4 to 5 hours later. The bay may have been related to a disturbance caused by a transient from a coronal mass ejection on 23 December. ULF Waves were produced later in the UTC day starting around 1900.

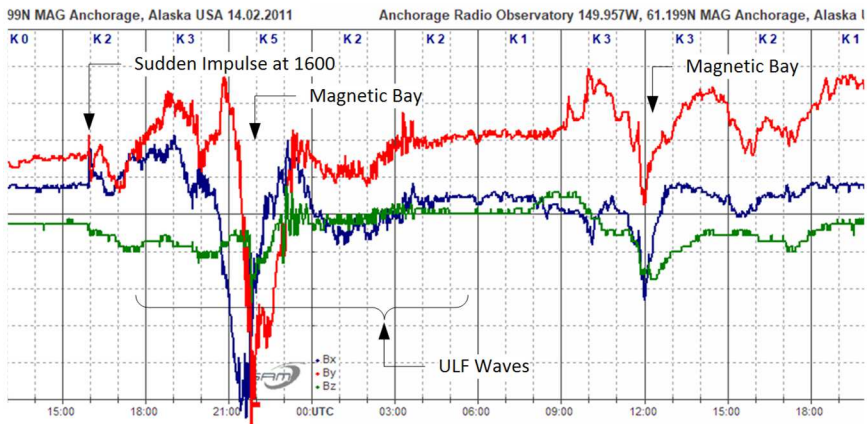


Figure 7.b ~ Magnetic bays on 14 & 15 February 2011. The first begins late in the UTC day on 14 February about 2030 and fully recovers 3 hours later. This bay is modulated by ULF Waves that extend about 5 hours into the following day. Another, less dramatic, bay is centered at 1200 on 15 February. Vertical scale is  $\pm 100$  nT and horizontal scale is time in UTC. The disturbance was caused by a coronal mass ejection that collided with Earth at 1600 on 14 February.

## I-2. ULF Wave Classifications

The terminology *ULF* used in the context of ULF Waves observed on a ground magnetometer is not to be confused with the similarly named electromagnetic (radio) band defined by the International Telecommunications Union. The ULF radio band is assigned the frequency range 300 to 3000 Hz with corresponding periods of 3.3 ms to 0.33 ms. However, in geospace physics, ULF Waves are defined as variations below a few Hz with corresponding periods longer than a couple hundred ms. ULF Waves are electromagnetic and those discussed here are the magnetic component recorded by a magnetometer. They typically are lower in frequency than the lowest radio band ELF (Extra- or Extremely-Low Frequency) of 3 to 30 Hz.

ULF Waves are divided into two basic types, *continuous* and *irregular*, based on how they appear in ground magnetometer records such as a *magnetogram*. The magnetogram is a plot of the measured magnetic flux density (magnetic induction) over time, usually 24 h. The continuous pulsations are quasi-sinusoidal lasting more

than several cycles (sometimes several hours) whereas the irregular pulsations are relatively short-lived. The frequency ranges and corresponding periods are listed in table 1.

Table 1 ~ ULF Wave Classifications

Type	Name	Frequency (mHz)	Period (s)
Continuous Pulsations	Pc 1	200 – 5000	0.2 – 5
	Pc 2	100 – 200	5 – 10
	Pc 3	22.2 – 100	10 – 45
	Pc 4	6.7 – 22.2	45 – 150
	Pc 5	1.7 – 6.7	150 – 600
Irregular Pulsations	Pi 1	25 – 1000	1 – 40
	Pi 2	6.7 - 25	40 – 150

The subtypes (Pc 1 through Pc 5 and Pi 1 and Pi 2) originally were assigned by a small subcommittee of the International Association of Geomagnetism and Aeronomy during 1963 [Jacobs] based on the spectra structural characteristics known at the time. However, additional types have since been found by spacecraft and terrestrial HF radars, such as SuperDARN, that are invisible to ground magnetometers. Now, the subtypes primarily indicate frequency bands and not so much wave structure. ULF Waves and their sources are not yet fully understood, but the two basic types and seven subtypes have stood the test of time and provide convenience for study.

The pulsations classified as irregular are characterized by their irregular form, close connection to disturbances of the magnetic field and correlation with upper atmosphere phenomena. ULF Waves of the two irregular subtypes form the microstructure of magnetic bays and similar disturbances seen during geomagnetic storms. According to [Jacobs], the microstructure of any geomagnetic disturbances can be built up from the subtypes. For example, pulsations during a sudden storm commencement (SSC) can be expressed as  $P_{SSC} = Pc\ 2 + Pi\ 1 + Pc\ 1$  and during a magnetic bay  $P_B = Pi\ 1 + Pi\ 2 + Pc\ 1$ . Pi 2 are pulsations usually associated with substorms and auroral brightening.

Studies have shown an association between Pc 3, Pc 4 and Pc 5 ULF Waves and the energization of radiation belt electrons, particularly at altitudes used by geostationary satellites (approximately 36 km). The direction of the IMF has been found to have some bearing on the generation of ULF Waves. When the IMF vector is within 50° of the Earth-Sun line, Pc 3 ULF Waves are observed on the ground, but if the IMF vector is roughly at a right-angle, they are not observed.

Pulsation amplitudes have been found to be proportional to solar wind speeds. When ULF Waves are observed, their amplitude but not their period varies with latitude. Usually, the wave amplitude peaks at some latitude, which is thought to be the latitude of the resonating magnetic field line. Latitudes of 60° to 70° map (that is, follow the magnetic field lines) from about the plasmapause to near the magnetopause on the dayside. Pc 5 ULF Waves with frequencies around 3 – 5 mHz (periods around 300 – 200 s) are common at these latitudes. The latitude at which the amplitude is largest varies with local time but remains between 60° to 65°. The observations discussed later are from Anchorage, Alaska, which is 62° north magnetic latitude.

Pc 5 waves with specific frequencies consistently appear in detailed spectral analyses and are called *magic frequencies*: 0.7, 1.3, 1.9, 2.6 – 2.7, 3.2 – 3.4, and 4.8 mHz. The frequencies vary a little depending on the type of

study, and they also wander slightly (a few tenths of mHz) over a solar cycle. Other frequencies also occur but those listed occur most often. Statistical studies show that these frequencies, or frequencies close to them, occur in the solar wind upstream of the magnetosphere as well as in the dayside magnetosphere and indicate that the solar wind is certainly the agency. The wavelengths of Pc3 to Pc5 waves are comparable to the size of the magnetosphere.

Several mechanisms have been concocted to explain the generation of discrete frequencies including monochromatic (single frequency) solar wind pressure variations, resonantly excited cavity waves, standing waves along magnetic field lines at the magnetopause and waveguide modes. The more current statistical studies conclude that *Periodic Density Structures* (PDS), or periodic fluctuations, in the solar wind directly drive some of the ULF Waves observed in the magnetosphere. However, not all frequencies are accounted for by PDS, and the processes still are being debated.

As described in the previous section, the Kelvin-Helmholtz waves are produced by shearing between the solar wind and magnetosphere. The threshold conditions for shear are met mainly in the regions that are on the dawn or dusk flanks of the magnetopause, so they may be the power source for ULF Waves observed during the local dawn or dusk. The dynamic pressure pulses in the solar wind are responsible for ULF Waves on the dayside noon region. It is thought that the power for Pc 4 and Pc 5 pulsations is supplied by solar wind pressure pulses, called *solar wind forcing*, that disturb the magnetosphere.

There have been reports that Pc 1 ULF Waves may act as precursors to seismic activity. There also are reports that Pc 1 pulsations present a potential hazard to certain types of heart conditions in humans and that some weekend Pc1 pulsations may be related to human activity or technology. However, these relationships have not yet been clearly established.

---

### I-3. Observatory & Instrumentation

Anchorage Radio Observatory is in a suburban location in Southcentral Alaska near the southern edge of the auroral oval (figure 8). The auroral oval is the footprint in the atmosphere where aurora is most likely to be seen. It marks the boundary between the highly concentrated magnetic field lines of Earth's polar cap and the more normal field lines at lower latitudes. The geographic coordinates of the Anchorage Radio Observatory are 61.20° N, 149.96° W. In 2022 the geomagnetic coordinates are 61.72 °N, 94.41 °W. At this location Earth's magnetic field has an inclination (or dip angle, the angle with respect to horizontal) of 74°.

L-shells frequently are used in discussions that involves the magnetosphere (figure 9). L-shells are idealized doughnut-shaped shells in Earth's magnetosphere that may be mapped from the ground to places in the magnetosphere where ULF Waves are produced. The L-shell number indicates the distance from Earth's center that a magnetic field line intersects Earth's equatorial plane and is defined in units of Earth radii (one Earth radii is approximately 6370 km).

Some specific types of phenomena occur most often at particular L-shells, so the concept allows a convenient reference to use in studies. For example, aurora is most often seen from the ground at latitudes that correspond to L = 6 but can reach L = 4 during moderate geomagnetic disturbances. During severe geomagnetic storms,

aurora may reach L = 2. The Van Allen radiation belts roughly correspond to L = 1.5 to 2.5, and L = 4 to 6. The L-shell may be calculated from

$$L = r / \cos^2(\lambda)$$

where  $r$  is distance from Earth's center in units of Earth radii and  $\lambda$  is the geomagnetic latitude. For ground observations,  $r = 1$ . The Anchorage Radio Observatory maps to the outer Van Allen radiation belt in the magnetosphere via L-shell 4.5 (figure 10 and 11).

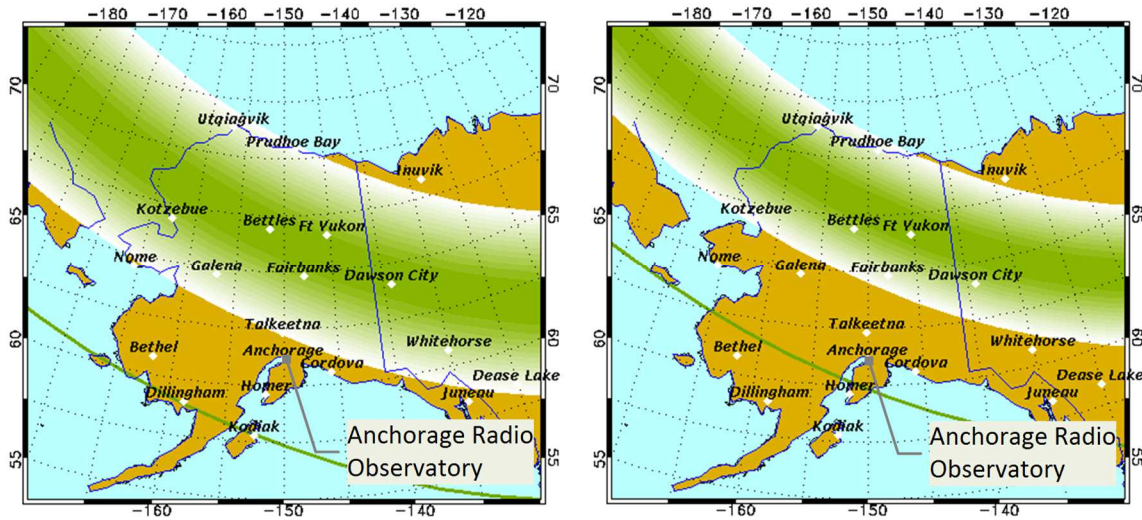


Figure 8 ~ Anchorage Radio Observatory shown with respect to the auroral oval (green gradient arc) during moderate geomagnetic activity (left) and low geomagnetic activity (right). When the magnetic field is highly disturbed, the auroral oval overlaps most of Alaska. These images were taken one day apart. Underlying image source: {UAFGI}

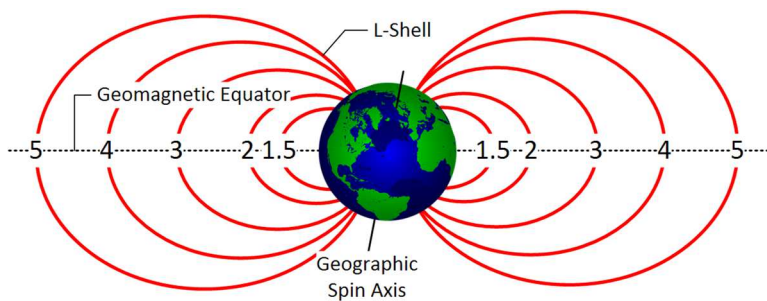


Figure 9 ~ L-shells surround Earth in an idealized donut shape of a dipolar magnetic field. The geomagnetic equator, shown as perfectly flat, also is idealized for purposes of illustration. The distortion of the magnetic field caused by the solar wind is not shown.

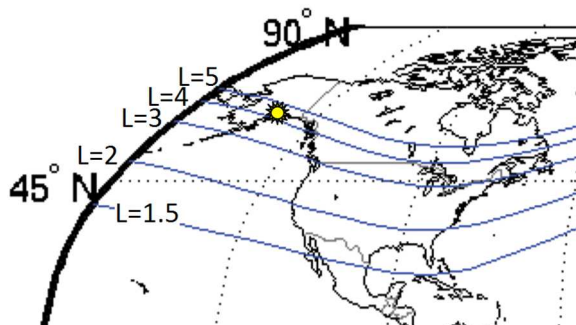


Figure 10 ~ Flattened map of North America showing the ground mapping of L-shells (light blue lines). Anchorage Radio Observatory is marked by the yellow star. The L-shells are warped with respect to geographic latitudes (45° and 90° N are marked by dotted lines) because Earth's dipole field is offset and tilted with respect to Earth's geographic spin axis. The ground location of the L-shells varies with geomagnetic conditions. Source: <https://en.wikipedia.org/wiki/L-shell>, author unknown

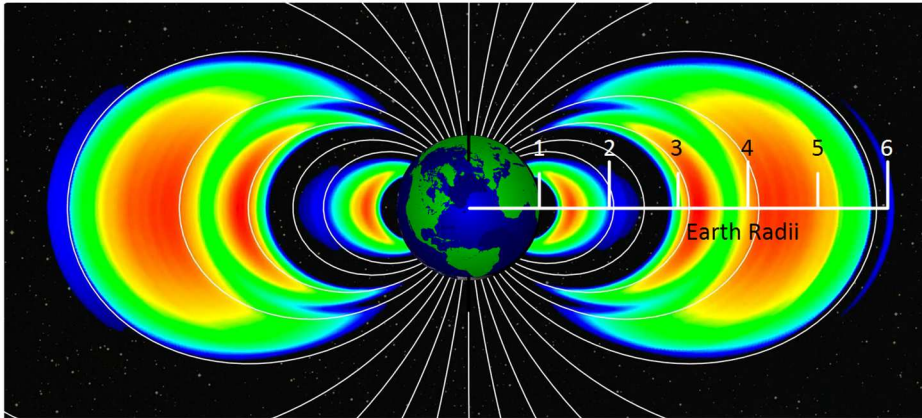


Figure 11 ~ Van Allen Radiation Belts scaled in Earth radii. Anchorage Radio Observatory is on L-shell 4.5, which maps to the most intense part of the outer radiation belt. The size and intensity of the belts vary considerably depending on the solar wind and related geomagnetic activity. Underlying image source: [\[NASA\]](#)

The SAM-III magnetometer consists of a main controller and three sensors (figure 12). Although it may be operated in stand-alone mode for portable applications, the SAM-III is most often connected to a PC, as it is at Anchorage Radio Observatory, for magnetogram display and data collection. The three sensors at Anchorage are oriented according to the Geographic Reference System: X-axis, true north-south; Y-axis, true east-west and Z-axis, vertical. The magnetometer is quite sensitive and can detect relatively low amplitude pulsations with a resolution of a couple nT.

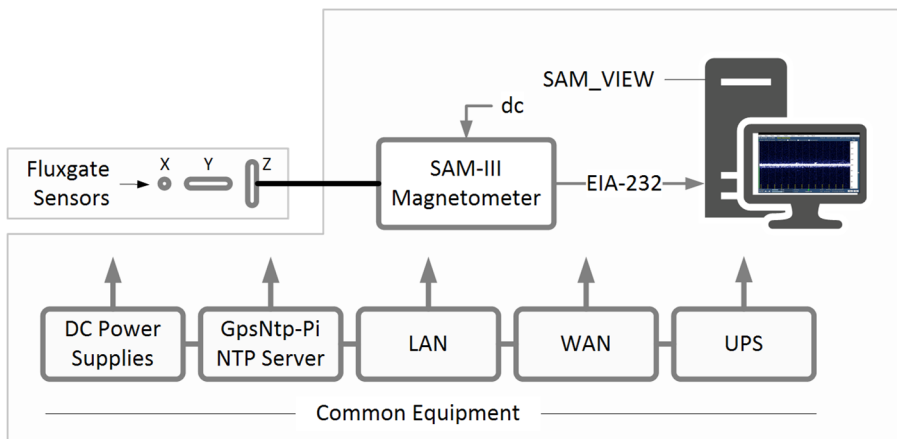


Figure 12 ~ SAM-III magnetometer at Anchorage Radio Observatory. The SAM\_VIEW software collects serial data from the SAM-III Controller at a 1/10 Hz rate. The three magnetic sensors are buried about 1 m below the ground surface to reduce the effects of daily temperature variations on sensor operation. Supporting equipment also is shown.

The SAM-III sample period is limited to the range 1 to 120 s or, equivalently, sample rates from 1 Hz down to 8.3 mHz. Based on the requirement that the sample rate be at least twice the highest frequency to be measured, the SAM-III can measure pulsations with alias-free frequencies no higher than 500 mHz to 4.3 mHz depending on the sample period setting. The Anchorage magnetometer is set to 10 s period, or 100 mHz sample rate, so its highest unaliased frequency is 50 mHz or periods longer than 20 s. Thus, the SAM-III potentially can detect Pc3, Pc4, Pc5, Pi1 and Pi2 type waves (see table 1).

The magnetometer's SAM\_VIEW software is the data collection program and runs on a Windows 10 x64 PC. It produces several types of files (table 2). The SAM-III includes other software applications for processing and viewing the data. These applications never alter the original data in any way.

Table 2 ~ SAM\_VIEW data files. Key: CSV: comma separated variable; CR/LF: carriage return/line feed; ASCII: American Standard Code for Information Interchange

<b>Contents</b>	<b>Format</b>	<b>File type</b>	<b>Time-stamp</b>	<b>Cadence</b>
Sensor data, X, Y and Z, CSV+CR/LF	Columnar	.txt (ASCII)	Yes	Real-time
Normalized sensor data (0000 UTC), CR/LF	Columnar	.sam (ASCII)	No	Real-time
Magnetogram	Image	.png	Yes	Real-time & daily
Records produced and any errors during the day	None	.log (ASCII)	No	Real-time & daily

---

## Part II-1. Observations

The observations took place throughout solar cycle 24 and the early part of cycle 25 (figure 13).

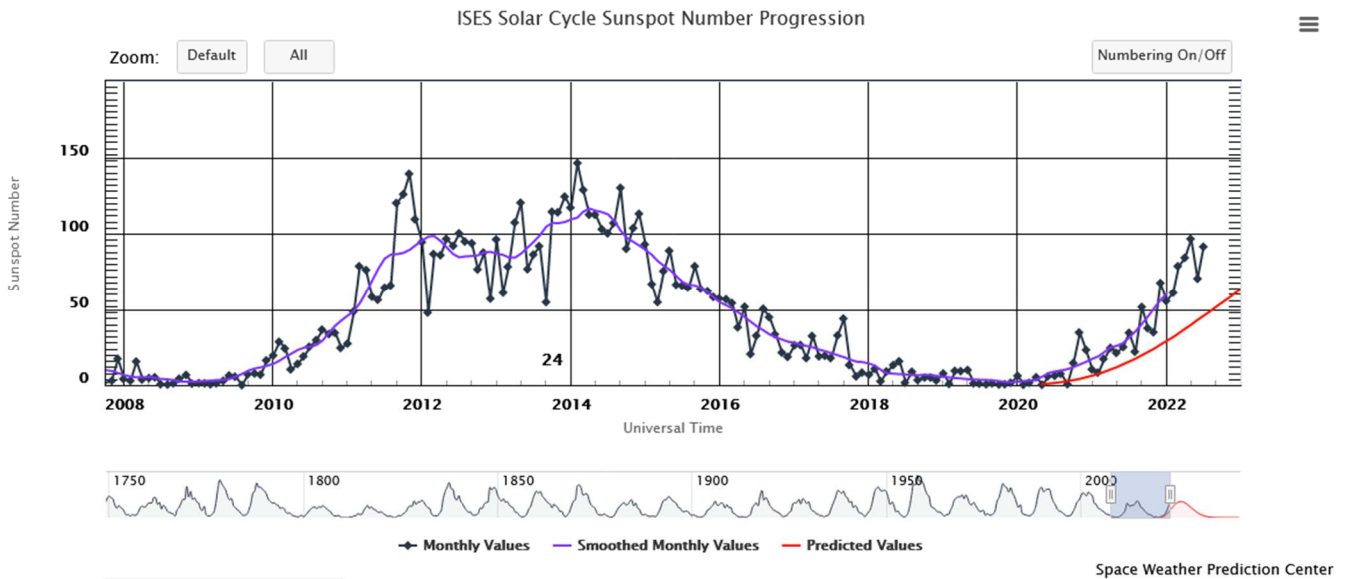


Figure 13 ~ Solar Sunspot Cycle 24 and the beginning of Cycle 25, the time period covered by this study. The lower scale and trace shows the sunspot cycles since 1750; the shaded area on the lower-right shows the range of the upper trace. Image source: [\[SWPC\]](#)

ULF waves are often observed on the Anchorage magnetograms as rapid oscillations on a relatively smooth background, most often on the X-axis (north-south) and Y-axis (east-west). They seldom are seen on the Z-axis (vertical). The phenomena are most easily recognized on relatively quiet days when the magnetogram traces do not show large deflections and the vertical scale on the magnetograms has not autoscaled to higher ranges. Many ULF Waves follow soon after the onset of disturbances caused by coronal hole high-speed streams (CHSS) and coronal mass ejections (CME) or a related sudden impulse.

Some geomagnetic phenomena most often occur at certain times of the day with respect to the Sun's position in the sky. A convenient time scale is based on the Sun's position in the sky with solar noon at 1200 and solar dusk at 1800. On the other hand, Coordinated Universal Time (UTC) is used for the time scale on all magnetograms for easy comparison across the globe. At Anchorage, solar noon (1200) is within a few minutes of 2200 UTC year-around. A lot of geomagnetic activity occurs due to reconnection in the magnetotail and is seen as variations in the X- or Y-axis magnetic flux density on magnetograms near local solar midnight (0000/2400) or 1000 UTC. The observations in this section include solar and UTC time scales (figure 14).

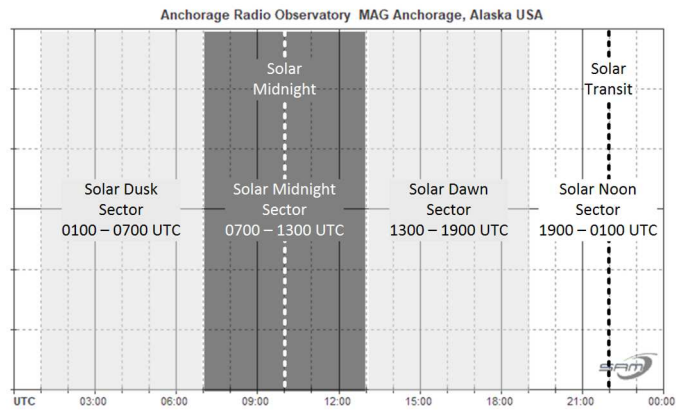
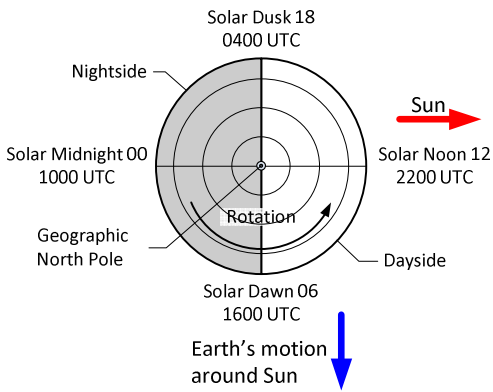


Figure 14 ~ Solar times and associated Coordinated Universal Times at Anchorage Radio Observatory. Left: Compact view of Earth as viewed from above along its rotation axis; the dawn and dusk sectors are not differentiated in this view. This view is shown as a quick reference for each observation in this section. Right: Magnetogram view showing each of the four sectors with 6 hours. This view provides a better perspective of the activity seen on the magnetograms in this section.

The magnetic records that show ULF Waves, and are discussed in this section, are thought to be representative but are far from complete. Observations are presented in chronological order from 2010 to 2022 as magnetograms and plots of specific time periods of interest and are summarized in tabular form (table 3).

Table 3 ~ Summary of observations discussed in this section

Figure	Date	Time (UTC)	Time (Solar)	Sector	Remarks
15	17 Dec 2010	1730-2100	0730-1100	Dawn-Noon	
16	6-7 Jan 2011	1800-0600	0800-2000	Dawn-Dusk	
17	14-15 Feb 2011	1730-0430	0730-1830	Dawn-Dusk	
18	18 Feb 2011	0130-0630	1530-2030	Dusk	
19	23 Dec 2014	1300-2100	0300-1100	Dawn +	
20	19-21 Dec 2015	1700-0400	0700-1800	Dawn-Dusk	
21	26 Dec 2015	1915-2300	0915-1300	Noon -	
22	31 Dec 2015-1 Jan 2016	1500-2300	0500-1300	Dawn-Noon	
		0000-1000	1400-2400	Noon-Midnight	
23	23 Jun 2016	1730-2400	0730-1400	Dawn-Noon +	
24	2 Aug 2016	1500-1730	0500-0730	Dawn	
		1930-2100	0930-2100	Noon -	
25	8 Feb 2017	1900-2030	0900-1030	Dawn-Noon	
26	10 Apr 2017	0130	1530	Noon-Dusk	
		1700-2030	0700-1030	Dawn-Noon	
27	28 May 2017	0330-1400	1730-0400	Dusk-Dawn	
28	23 Jan 2018	2000-2030	1000-1030	Dawn-Noon	ULF unlikely
29	15 Feb 2018	1630-2400	0630-1400	Dawn-Noon +	
30	16 Feb 2018	0000-2400	1400-1400	All	24 h
31	30 Nov 2019	1830-2400	0830-1400	Noon -	
32	30 Nov-1 Dec 2019	1830-0400	0830-1800	Noon-Dusk	
33	10 Dec 2020	0200-0500	1600-1900	Dusk	
34	12 May 2021	1200-1600	0200-0600	Midnight-Dawn	
35	27 Aug 2021	1700-2100	0700-1100	Dawn-Noon	
36	17-18 Aug 2022	1630-1800	0630-0800	Dawn	
		2100-2400	1100-1400	Noon	

All original data are discrete time series with 10 second sample interval. Some events are transformed to the frequency domain using the Fast Fourier Transform (FFT) Analysis tool in Excel. The transformations were performed on the horizontal (H-) component, which is the vector sum of the X- and Y-components. It was found that the frequencies found in the FFT analysis for any given event varied with the length of the data. The dataset lengths are directly proportional to the time spans being analyzed, and it is likely the ULF Wave spectra changed in the longer time intervals.

The frequency resolution of the FFT is determined from the bin size defined by  $f_s/N$ , where  $f_s$  is the sampling rate and  $N$  is the number of datapoints (always a power of 2). The Anchorage SAM-III is set to 100 mHz sampling rate, so the resolution in mHz is  $100/N$  in the Anchorage data. For example, at 1024 point dataset has 0.1 mHz resolution and a 4096 point dataset has 0.02 mHz resolution. The transformation procedures are given in the Appendix. Several events were manually analyzed by visually counting the cycles and then converting to frequency, a method that yields only averages and is somewhat subjective.

Several frequencies or range of frequencies repeatedly appear in the FFT plots. Some indications may be noise or instrumental effects rather than actual spectra (see Discussion in the next section).

2010 ►

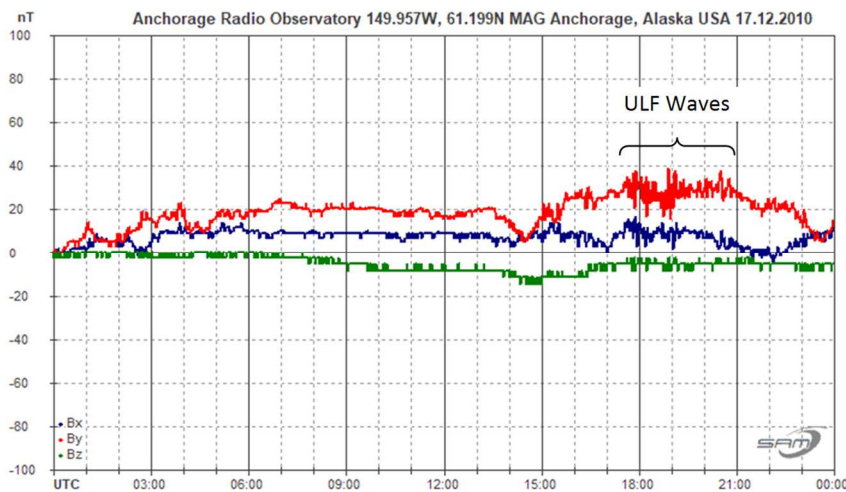
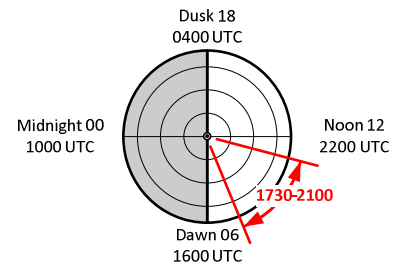


Figure 15.a ~ Quiet magnetic day with ULF Waves starting about 1730 on 17 December 2010.



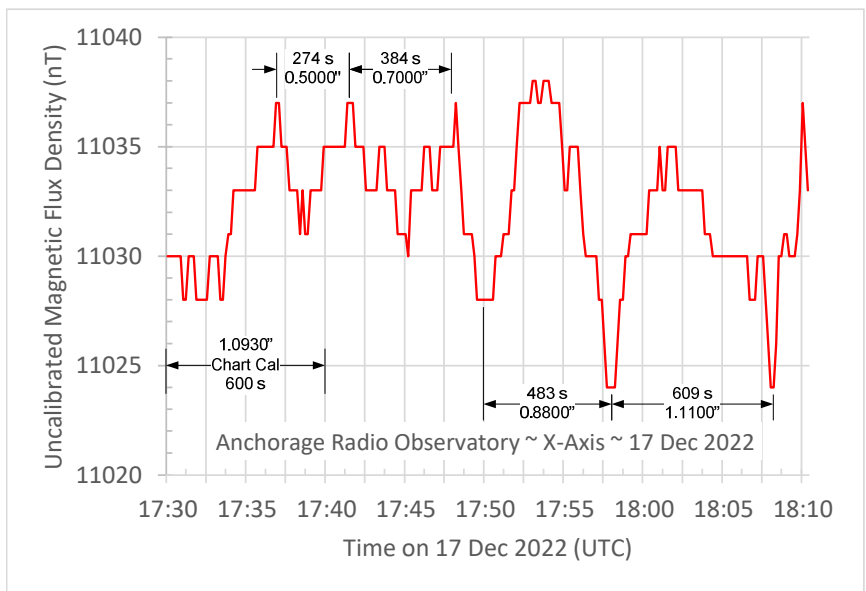


Figure 15.b ~ ULF Waves indicated above. These waves are quasi-periodic with periods from 274 s to 600 s over a 35 min time span, or 3.7 to 1.7 mHz.

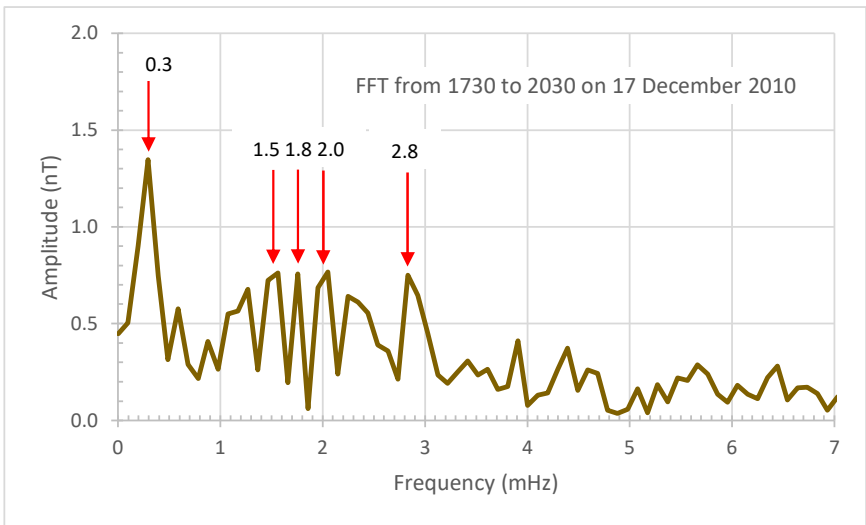


Figure 15.c ~ 1730 to 2030 on 17 December 2010. Possible Pc1 at 0.3 mHz (3333 s period) but may be noise.

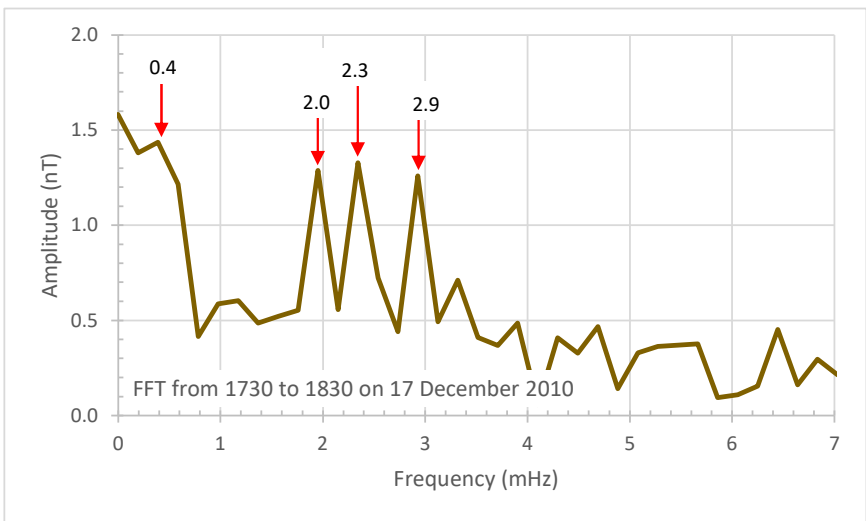


Figure 15.d ~ 1730 to 1830 on 17 December 2010.

2011 ▶

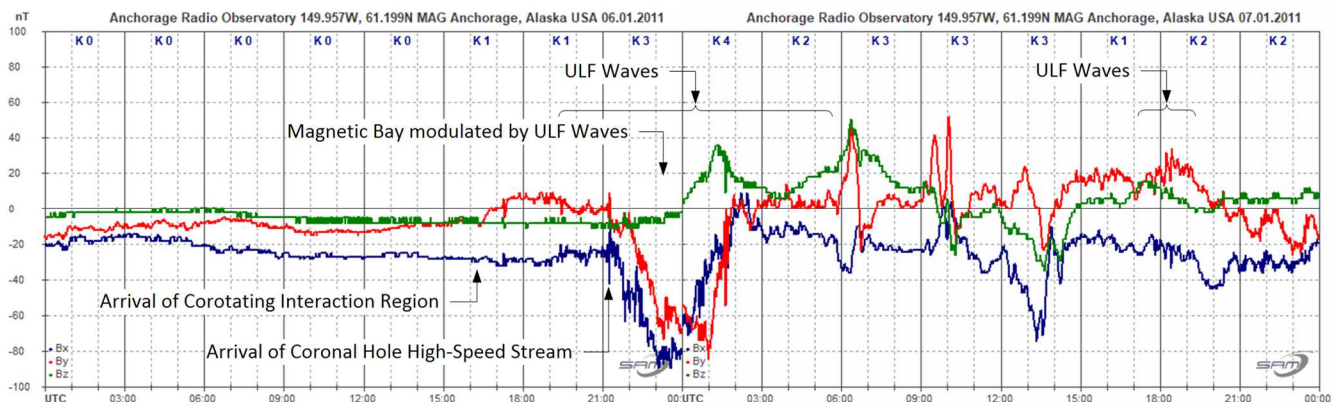


Figure 16.a ~ Magnetograms from two consecutive days, 6 and 7 January 2011, spliced together to show development of a mild geomagnetic disturbance (note K-index values) from a coronal hole high-speed stream that produced ULF Waves.

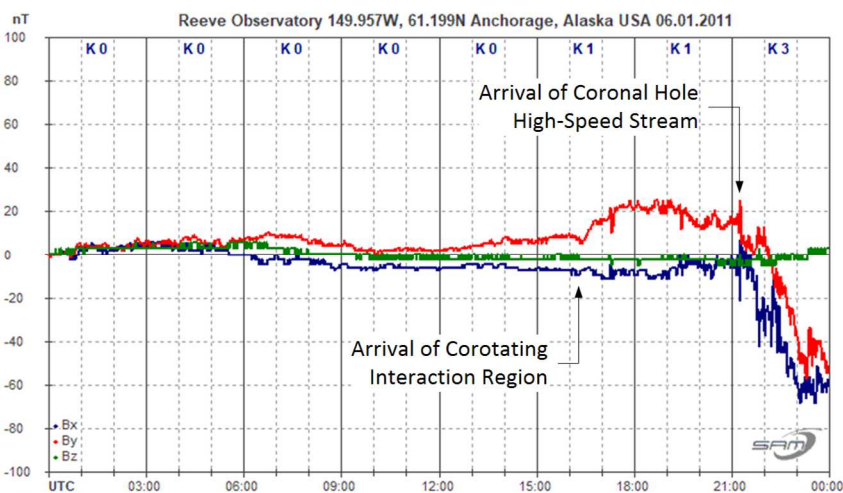


Figure 16.b ~ Example of pulsations modulating a magnetic bay that started at 2100 upon arrival of a coronal hole high-speed stream. The bay starts to recover around 2330-2400 but the magnetic field continues to be unsettled for at least 24 h.

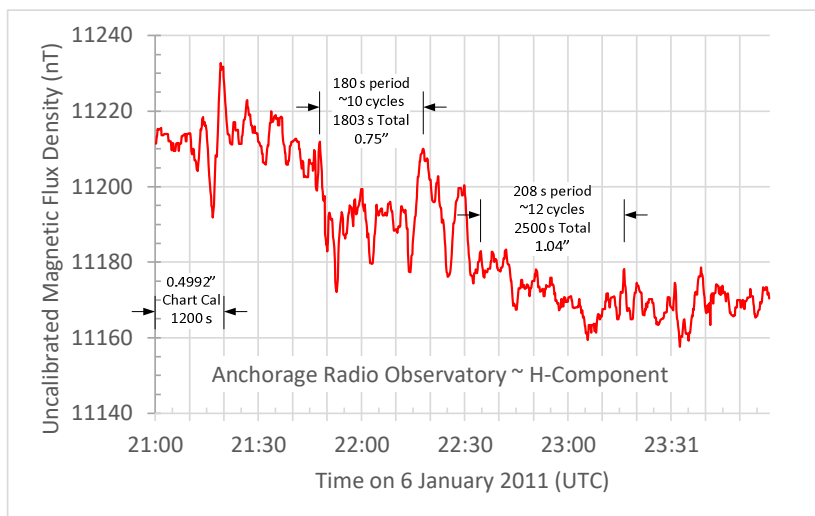
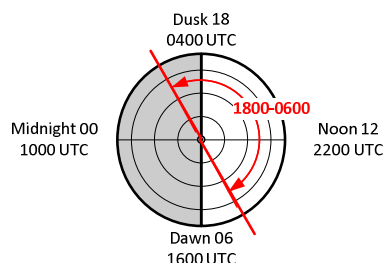


Figure 16.c ~ ULF Wave indicated above on 6 January from 2100 to 2400. This wave rides on a magnetic bay. Two parts of the trace were measured and showed periods of 180 to 208 s corresponding to Pc 5 ULF Waves. The approximate average period for the entire 4 hours by hand counting all positive peaks is 261 s or 3.8 mHz (55 cycles over 14 400 s).

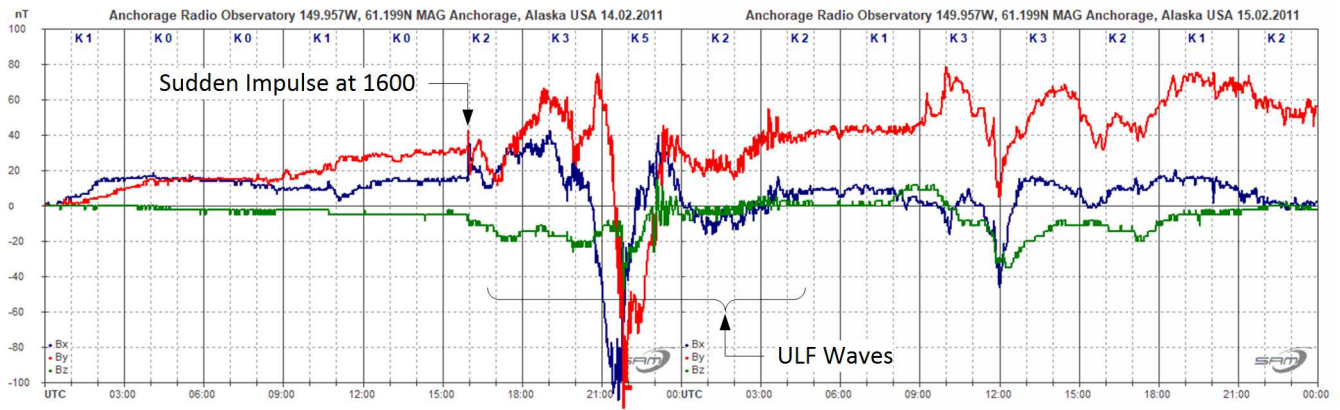


Figure 17.a ~ Magnetograms from two consecutive days, 14 and 15 February 2011, spliced together to show development of a moderate geomagnetic disturbance (note K-index values) from a sudden impulse at 1600 and associated coronal mass ejection. This disturbance produced sustained ULF Waves that lasted about 12 hours from 1630 on 14 February to 0430 on 15 February.

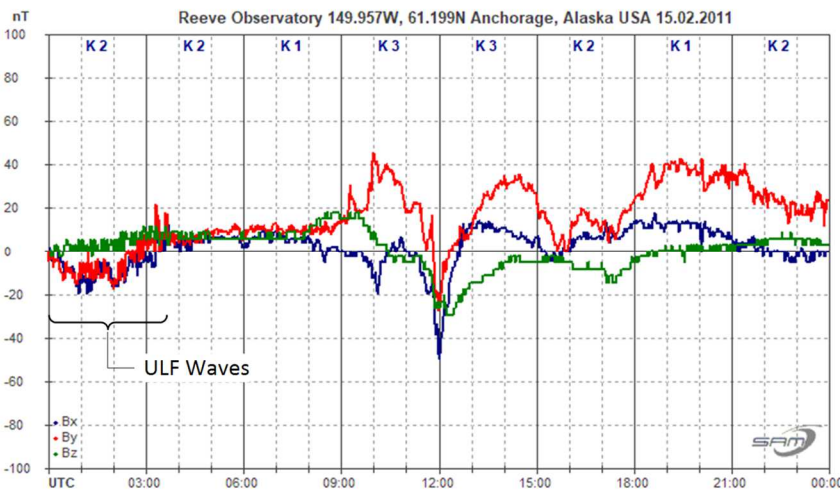


Figure 17.b ~ Higher detail of ULF Waves following a sudden impulse and a brief period of geomagnetic storm (K5) on 15 February.

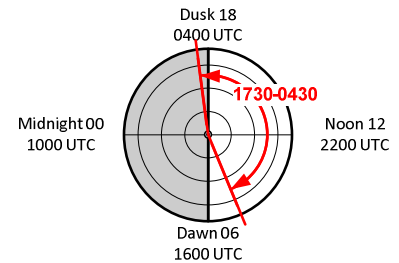
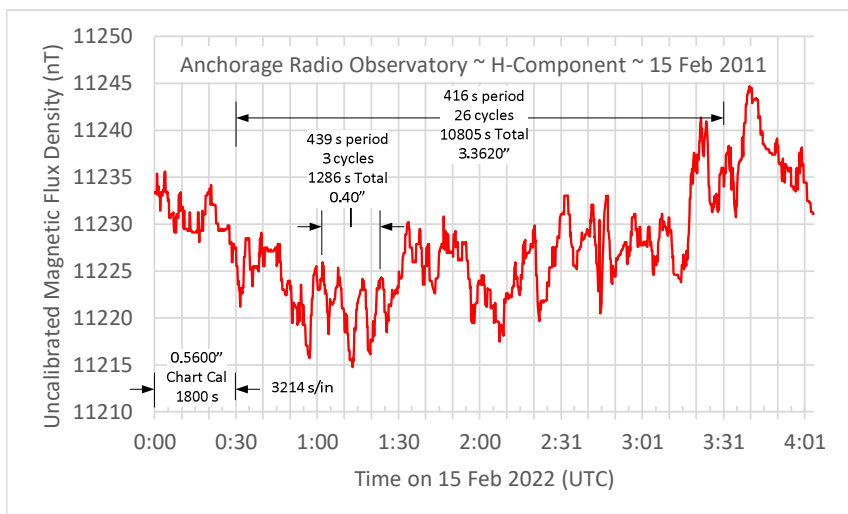


Figure 17.c ~ ULF Waves indicated above from 0000 – 0400 on 15 February. The average period over a 1 h time span is 416 s, or 2.4 mHz. A shorter sample of 3 cycles has an average period of 439 s. This wave appears to have some shorter and longer period components but they were not analyzed.



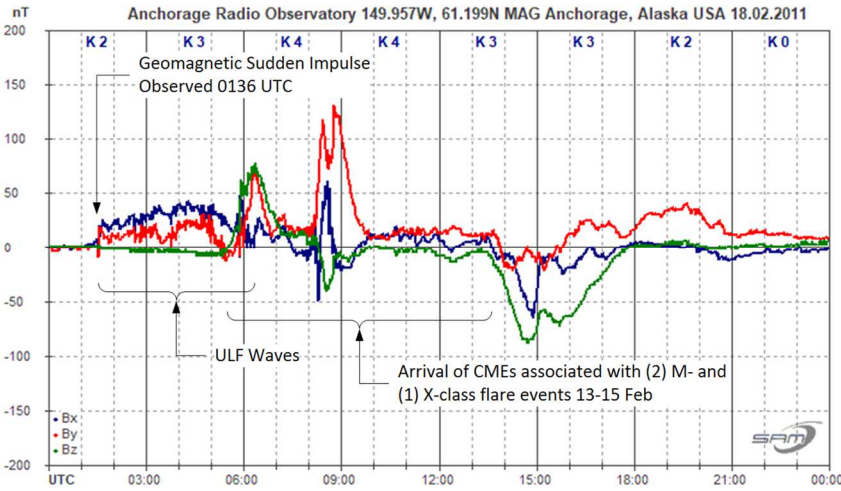
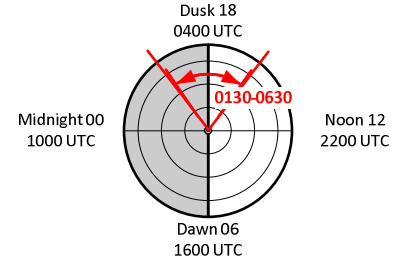


Figure 18 ~ ULF Waves immediately following a sudden impulse on 18 February 2011 that was associated with two M- and one X-class x-ray flares. The ULF Waves lasted about 4.5 hours.



2014 ▶

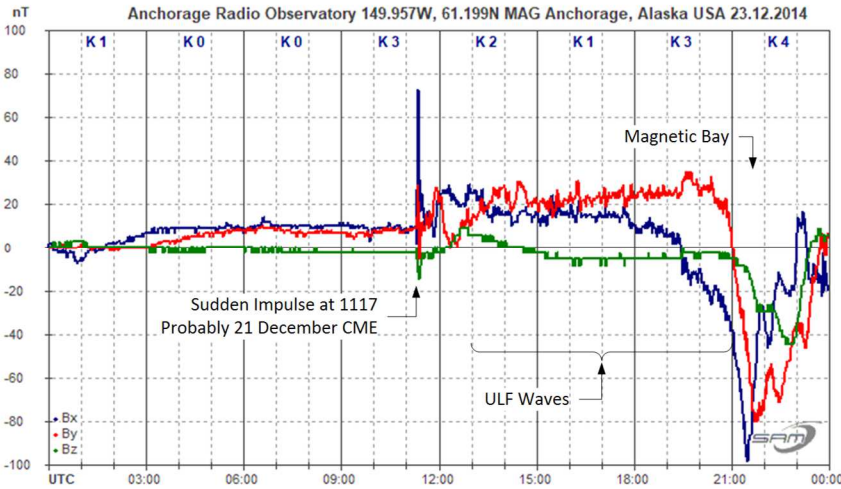
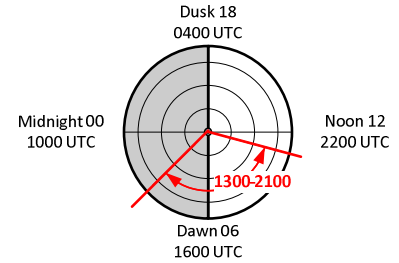


Figure 19 ~ ULF Waves following a sudden impulse on 23 December 2014. Magnetic bay starting as early as 1900 in X-component but delayed until 2100 in Y- and Z-components.



2015 ▶

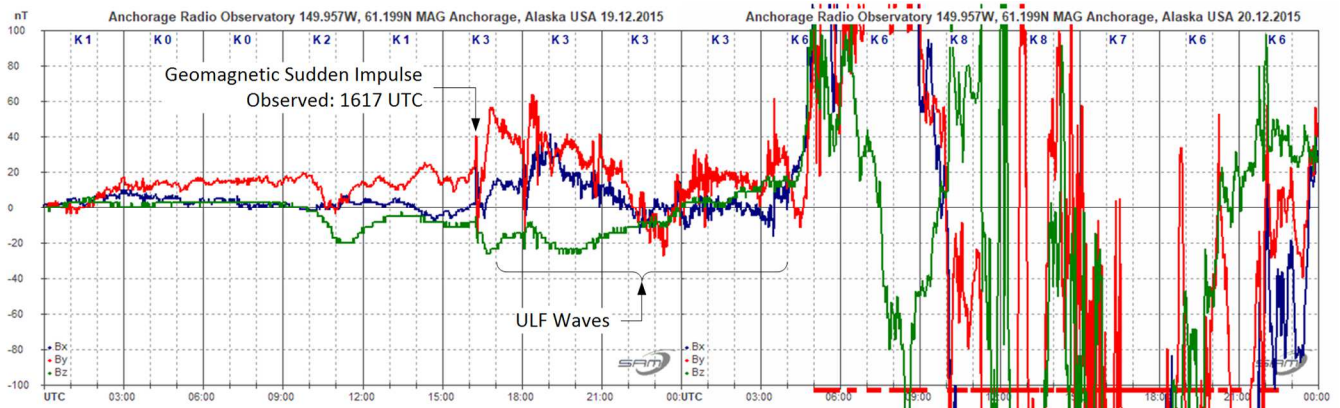


Figure 20.a ~ Initial development of a strong geomagnetic storm that started on 19 December 2015 and extended through 21 December. This image consists of two magnetograms spliced together and with a fixed vertical scale to better show the sequence of events. A sudden impulse was observed at 1617 on 19 December, which produced ULF Waves from about 1700 on 19 December to 0400 the next day. Storm conditions were reached immediately after the ULF Waves appear to have subsided. It is possible ULF Waves have been hidden by the strong deflections during the storm. Note the vertical scale is  $\pm 100$  nT.

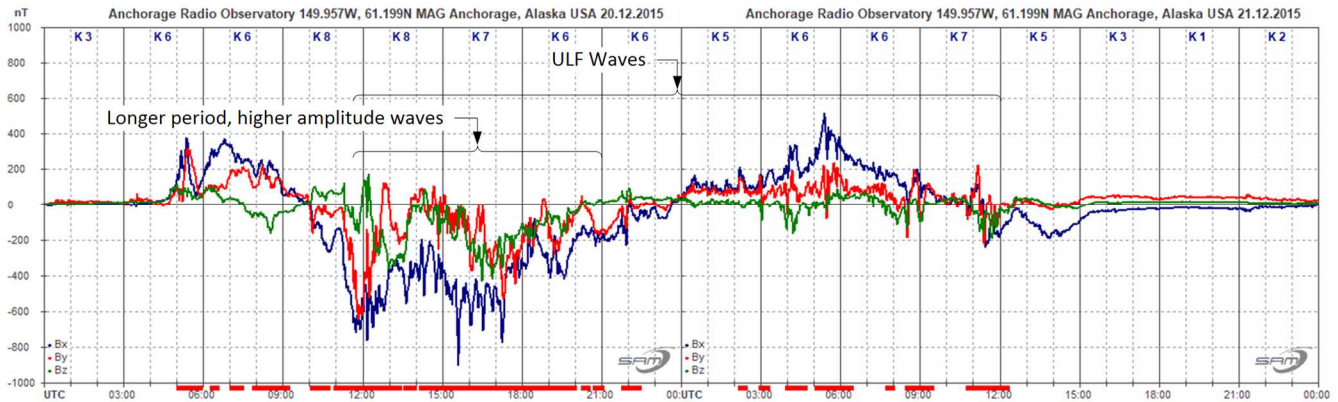
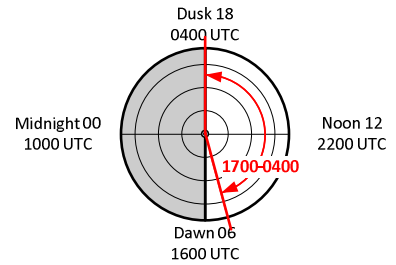


Figure 20.b ~ Continuation of the geomagnetic storm that started on 20 December from a 19 December sudden impulse (see previous magnetogram). Note the vertical scale is now  $\pm 1000$  nT. This image also consists of two magnetograms spliced together and with a fixed vertical scale. As mentioned above, the storm conditions were reached about 0400 on 20 December. Another long interval of ULF Waves started before 1200 that day and continued through to 1200 on 21 December. There also was 9 hour interval during which longer period waves dominated the magnetograms, from about 1200 to 2100 on 20 December. The disturbance finally quieted down around 1500 on 21 December.

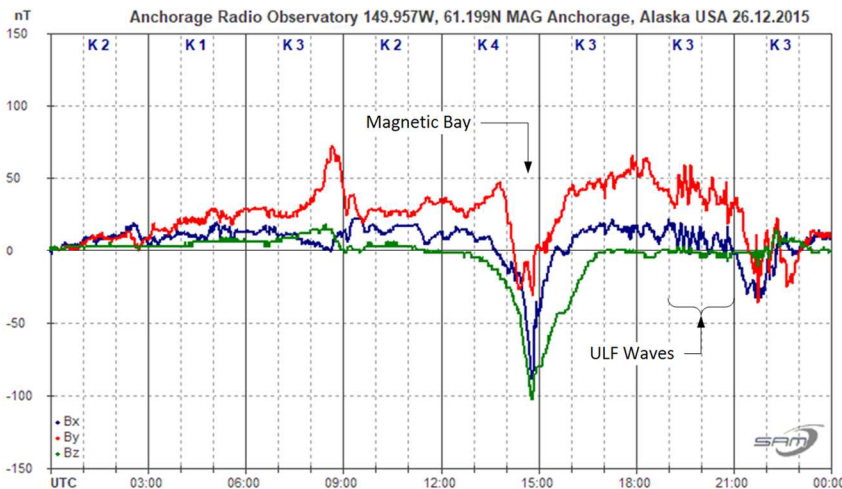
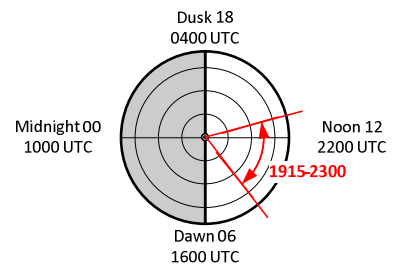


Figure 21 ~ A magnetic bay occurred on 26 December 2015 at around 1400 and was followed 5 hours later by ULF Waves at 1900. The waves lasted about 2 hours.



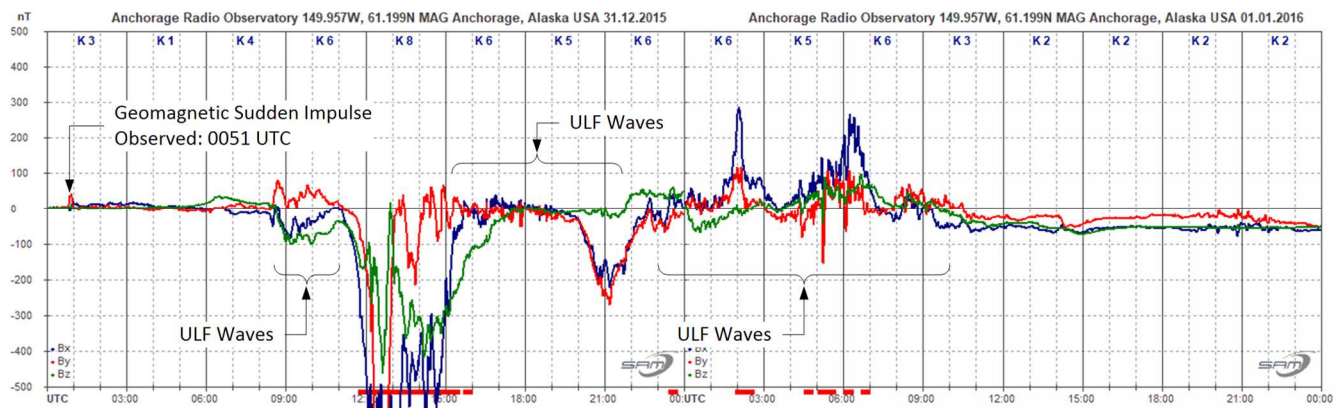


Figure 22 ~ Storm conditions and ULF Waves followed a sudden impulse at 0051 on 31 December 2015. These are shown on two magnetograms spliced together for 31 December 2015 and 1 January 2016. Storm conditions were reached during the 0900-1200 synoptic period coincidental with the ULF Waves on 31 December. The wild geomagnetic deflections during the next synoptic period may have buried additional ULF Waves. They become visible again at about 1500 and continue for almost 7 hours. After a brief quiet period, additional ULF Waves appear around 2300 and extended into 1 January until 0400.

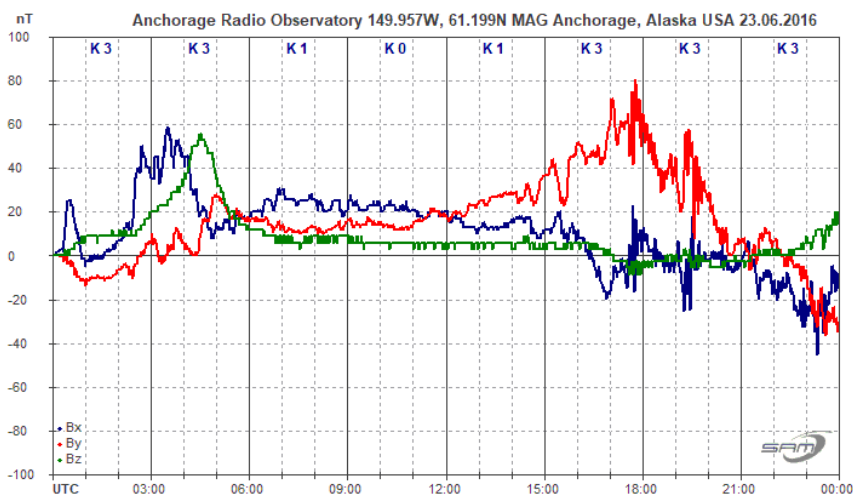
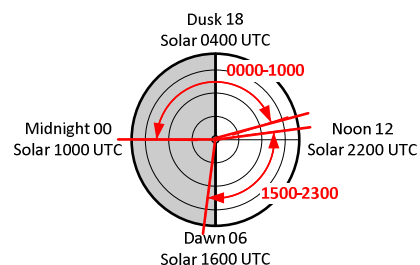
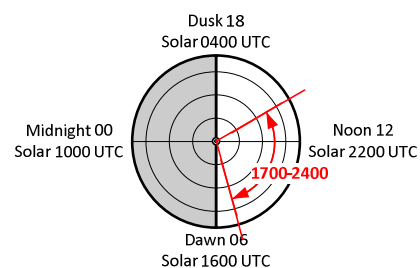


Figure 23 ~ ULF Waves are seen starting about 1730 on 23 June 2016 and lasting through the end of day. The magnetogram for 24 June (not shown) indicates the ULF waves continued for several more hours.



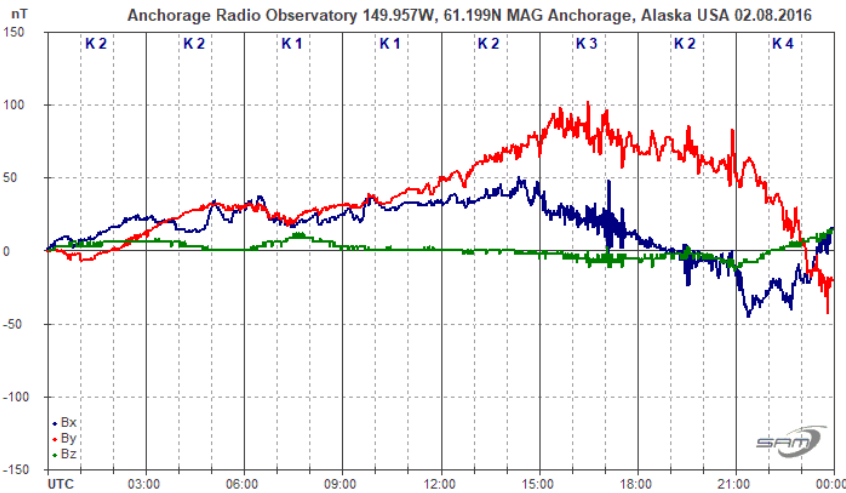
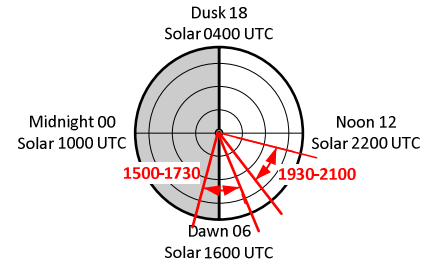


Figure 24 ~ In this magnetogram for 2 August 2016, ULF waves start around 1400 and continue through at least the end of day.



2017 ▶

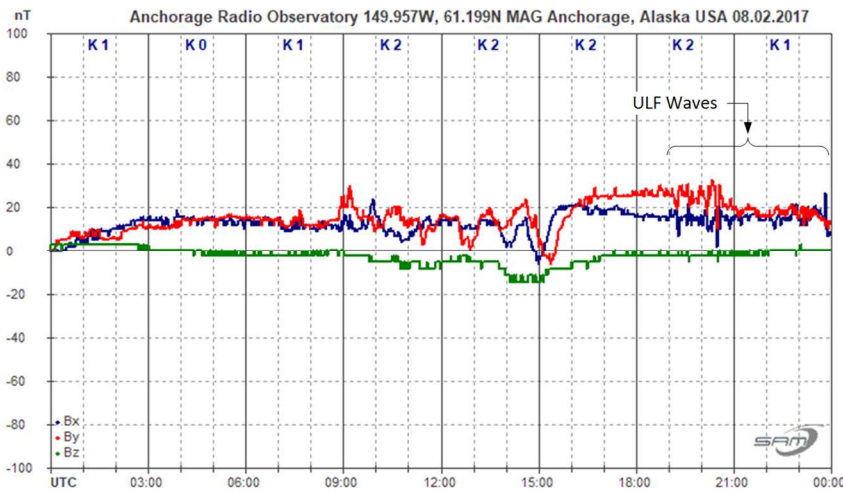


Figure 25 ~ The magnetic field is unsettled throughout 8 February 2017 but there are no storm conditions. ULF Wave start about 1900 and continue through at least the end of day.

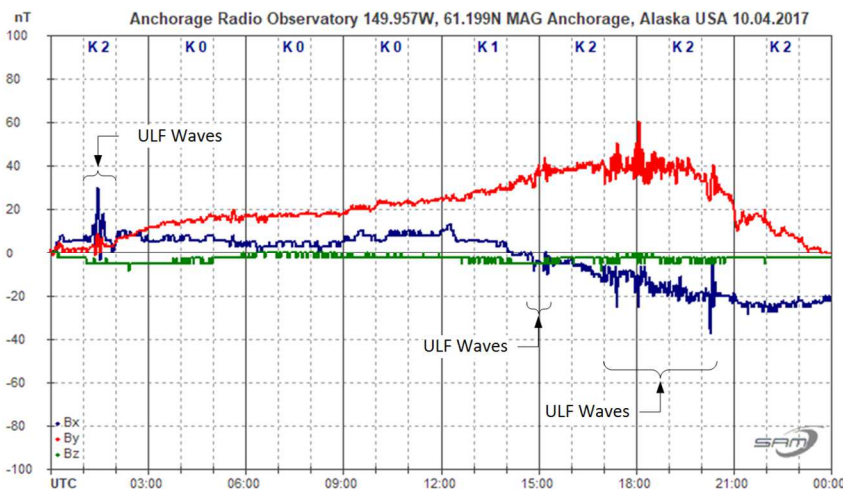
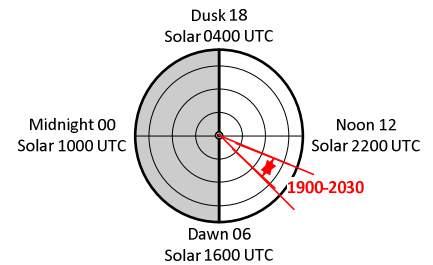
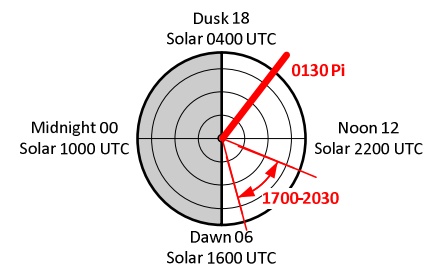


Figure 26.a ~ Two short pulsation intervals appear around 0130 and 1500 (both shown in detail below) on 10 April 2017. Continuous pulsations occur between about 1700 and 2030.



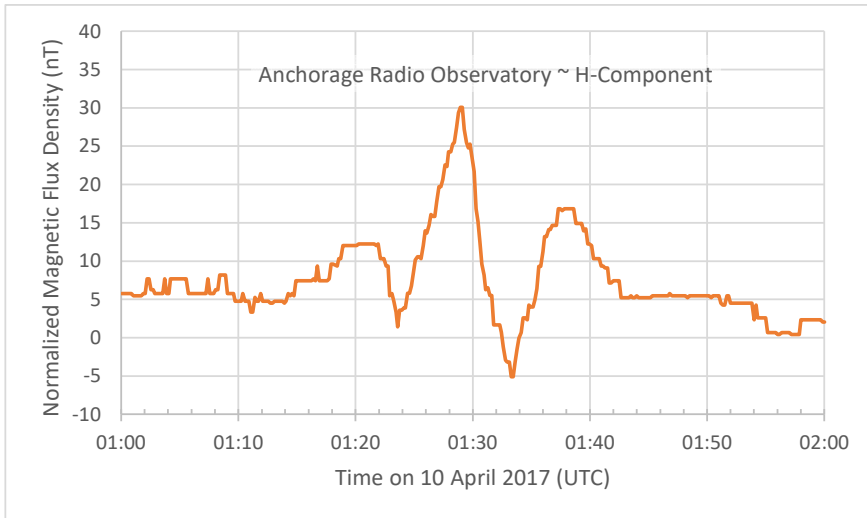


Figure 26.b ~ Two relatively large pulsation cycles seen on above magnetogram around 0130 lasting 18 min. The average period is 540 s, equivalent to 1.9 mHz. These may be Pi; however, preceding the large pulsations are much weaker pulsations. The 10-minute interval from 0102 to 0112 contains 8 weak cycles, or an average period of 12.5 s, equivalent to 0.8 Hz, which correspond to Pi 1.

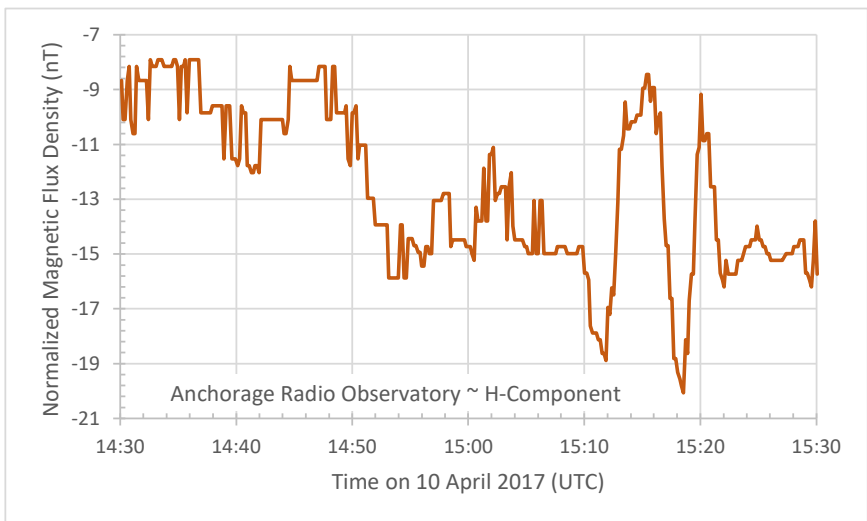


Figure 26.c ~ Continuous pulsations dominate this short 1 hour record from 1430 to 1530 on 10 April 2017. The pulses from 1430 to 1510 have an average period of approximately 59 s, equivalent to 17 mHz and Pc 4 classification. There also are irregular pulsations. The longest pulse starting at 1500 has a period of 420 s, equivalent to 2.3 mHz. The following pulse starting at 1517 has a period of 360 s, equivalent to 2.8 mHz.

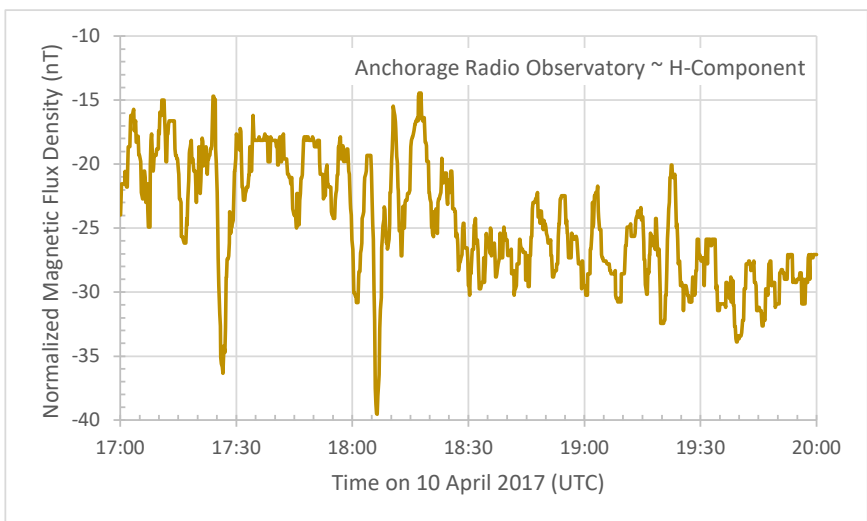


Figure 26.d ~ Continuous pulsations from 1700 to 2000 on 10 April 2017. There are approximately 61 cycles during the 10 800 s shown with an average period of 177 s, equivalent to 5.6 mHz.

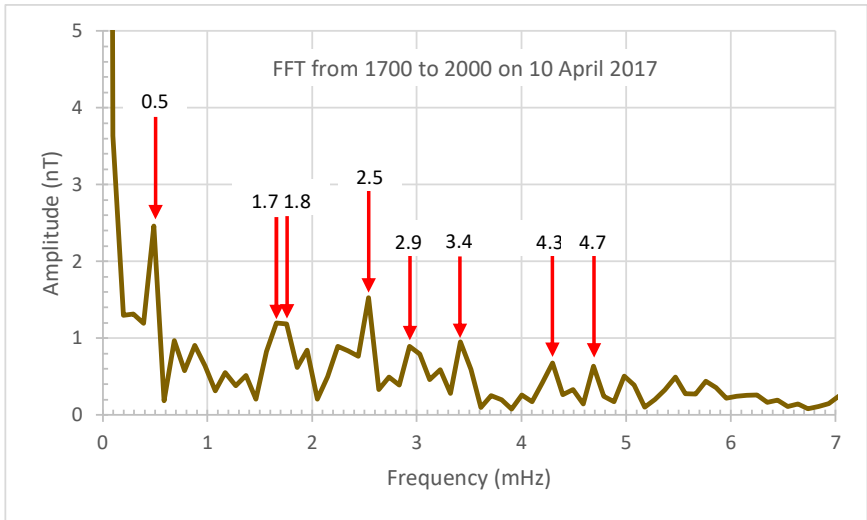


Figure 26.e ~ FFT absolute magnitude on vertical scale against frequency of 1024 data elements for the time period 1700 to 2000 UTC on 10 April 2017.

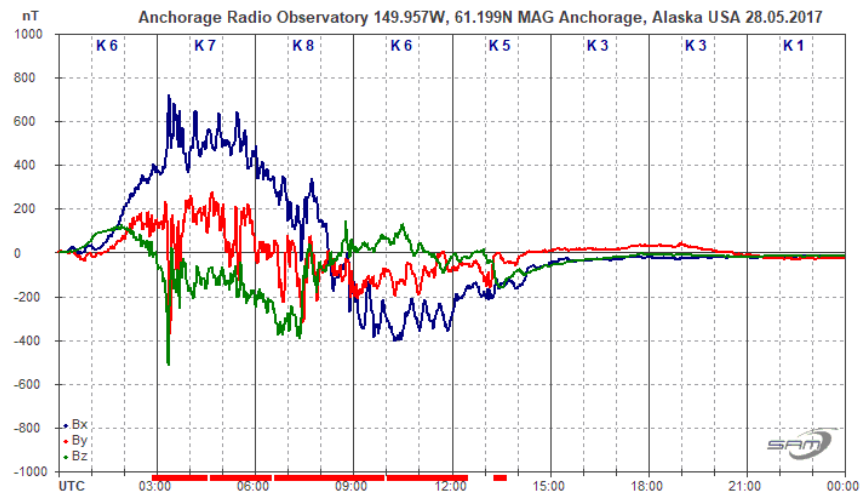
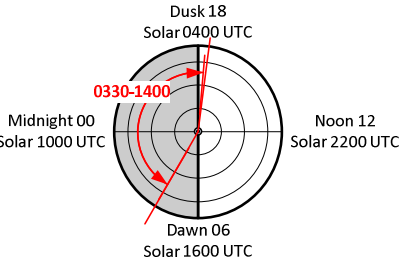


Figure 27 ~ Geomagnetic storm conditions occur on 28 May 2017 during the first synoptic period and last for over 12 hours. Strong pulsations are obvious after 0300 but their period has not been measured. Long period structures can be seen between 0900-1200.



2018 ▶

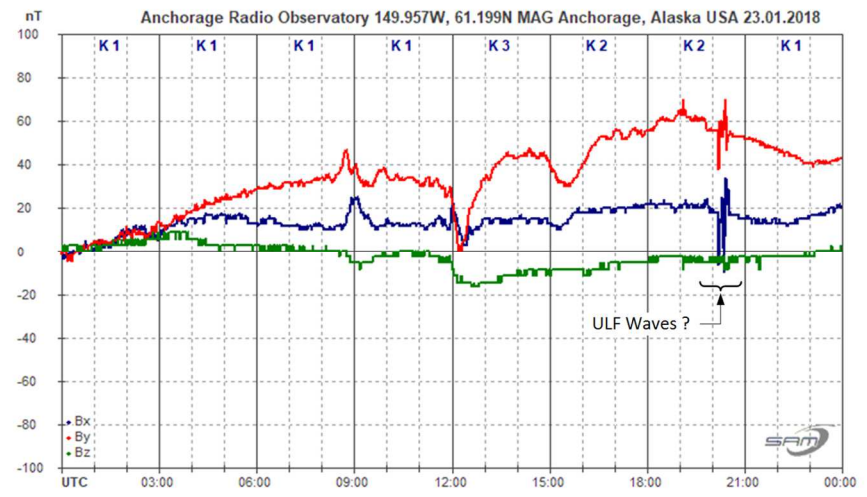
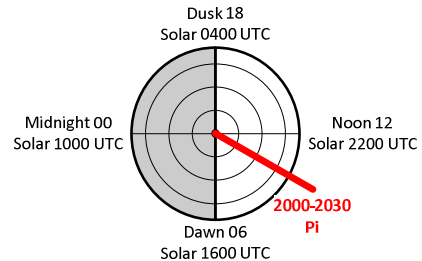


Figure 28.a ~ Example of irregular pulses on 23 January 2018 that probably are not ULF Waves. The pulsations occur at about 1715 and last for about 15 min. The source is unknown but probably road maintenance equipment or a delivery truck driving nearby. See below for more detail.



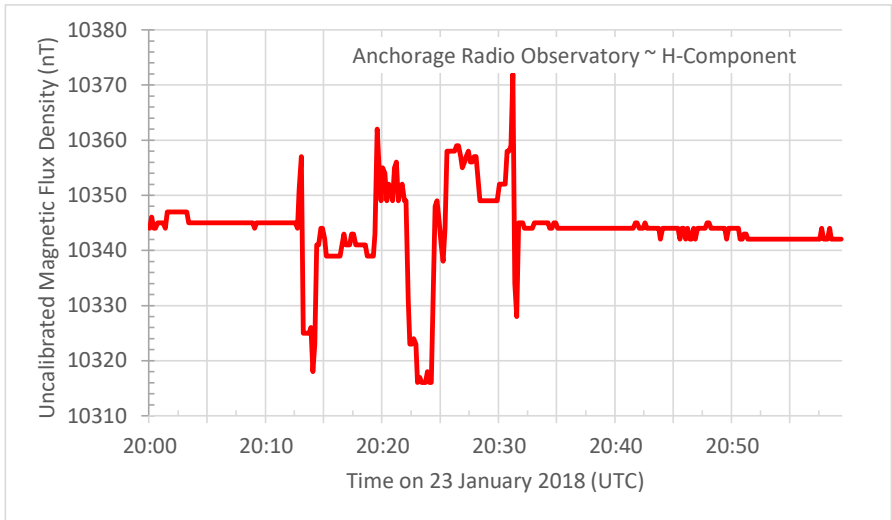


Figure 28.b ~ The pulsations seen on the 24 hour magnetogram above may have been caused by road traffic as indicated by their sharp transitions and spikey nature.

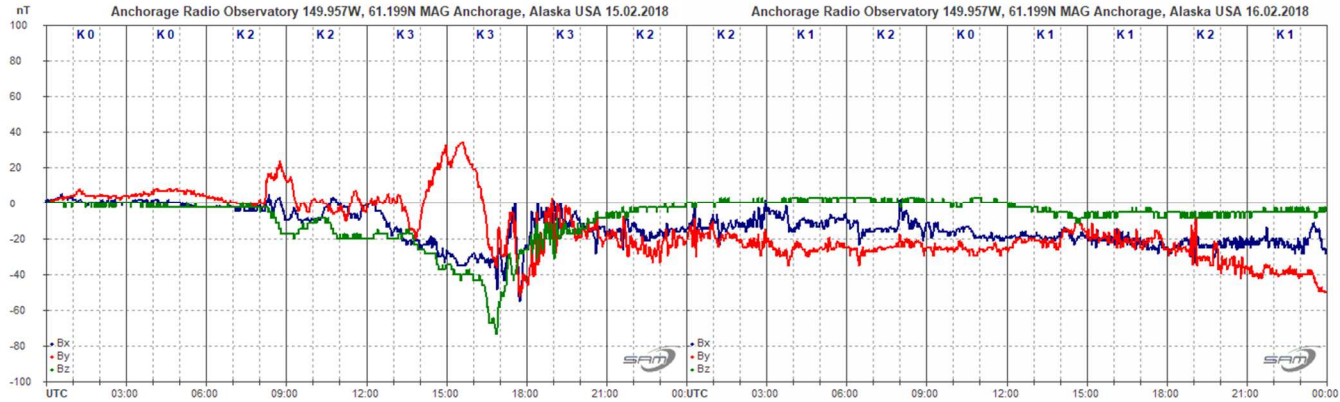
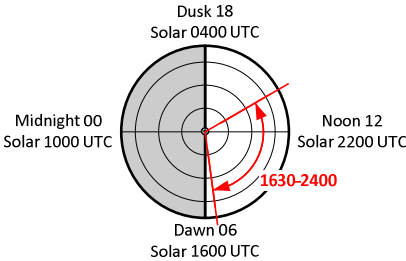


Figure 29 ~ Two 24 hour magnetograms have been spliced together to show ULF Waves that appear to start about 1700 on 15 February 2018. They continue through the next day, weaken around 0300 but strengthen again at about 1500. The enhanced interval lasts until at least 2100. These waves were apparently induced by the arrival on 12 February of a coronal mass ejection that had mostly positive (northward) Bz component.



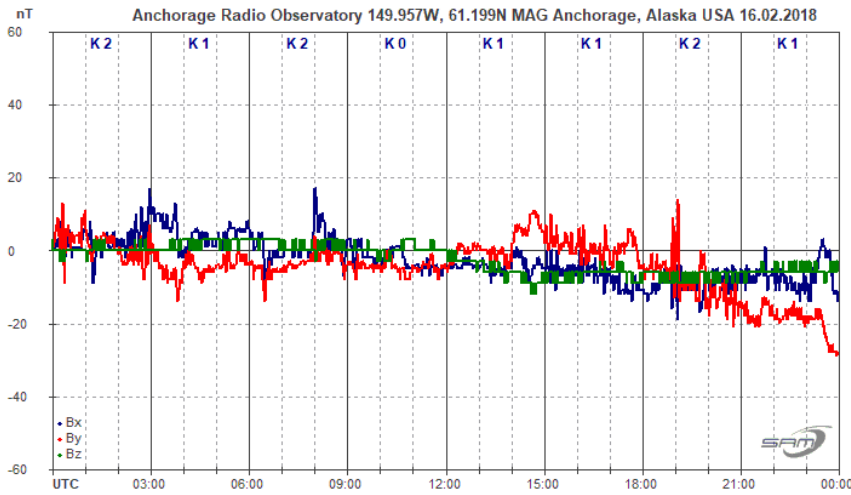


Figure 30.a ~ This 24 h magnetogram from 16 February 2018 appears to show ULF Waves. However, FFT analysis indicates that only low amplitude oscillations are present and more likely are noise. Note the scale is  $\pm 60$  nT compared to  $\pm 100$  nT in the previous magnetograms.

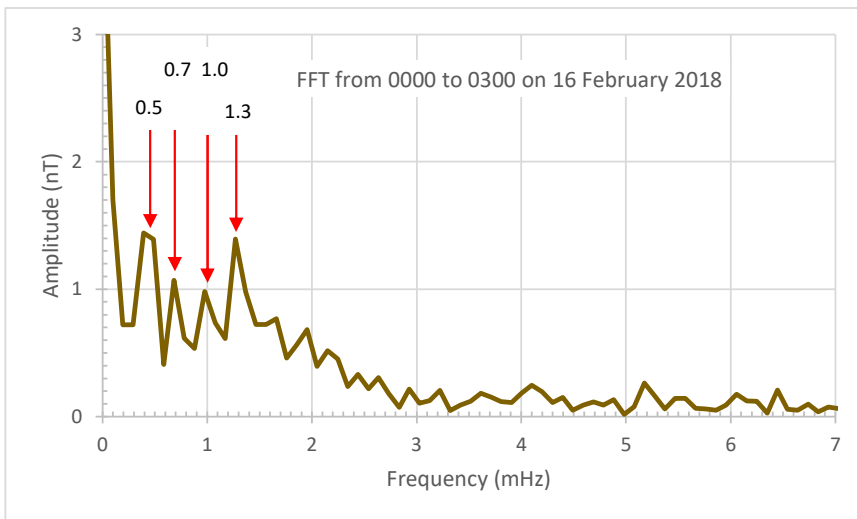
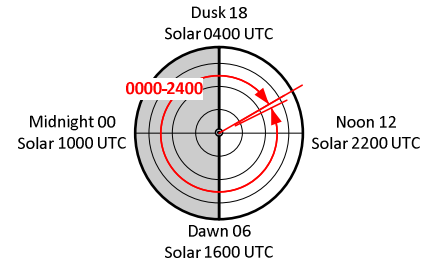


Figure 30.b ~ FFT of data from 0000 to 0300 on 16 February 2018 using 1024 datapoints. Although several frequencies are annotated, they signal amplitudes are low and probably noise.

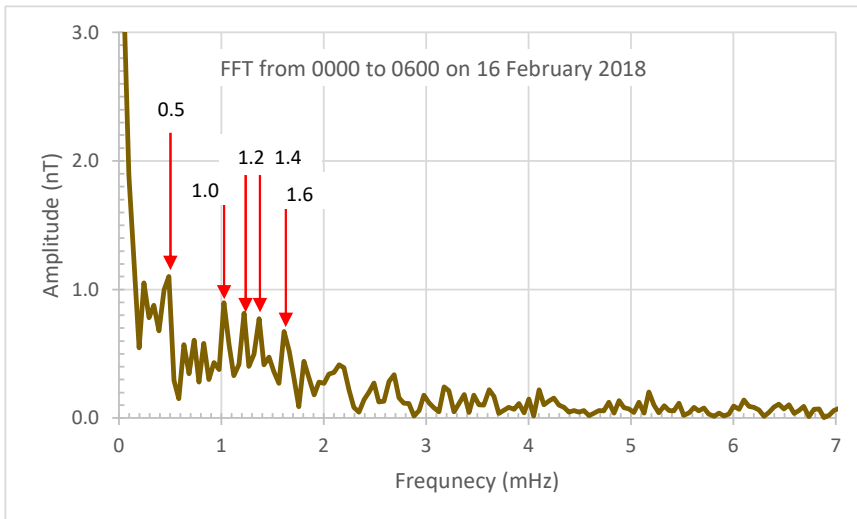


Figure 30.c ~ FFT of data from 0000 to 0600 on 16 February 2018 using 2048 datapoints. Although several frequencies are annotated, the signal amplitudes are low and probably noise.

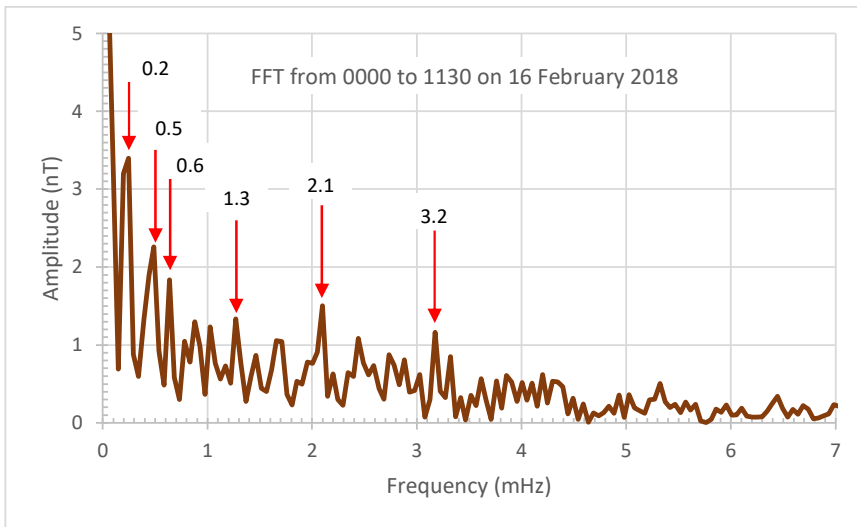


Figure 30.d ~ FFT of data from 0000 to 1130 on 16 February 2018 using 4096 datapoints. Although several frequencies are annotated, the signal amplitudes are low and probably noise except for 0.2 mHz (5000 s period).

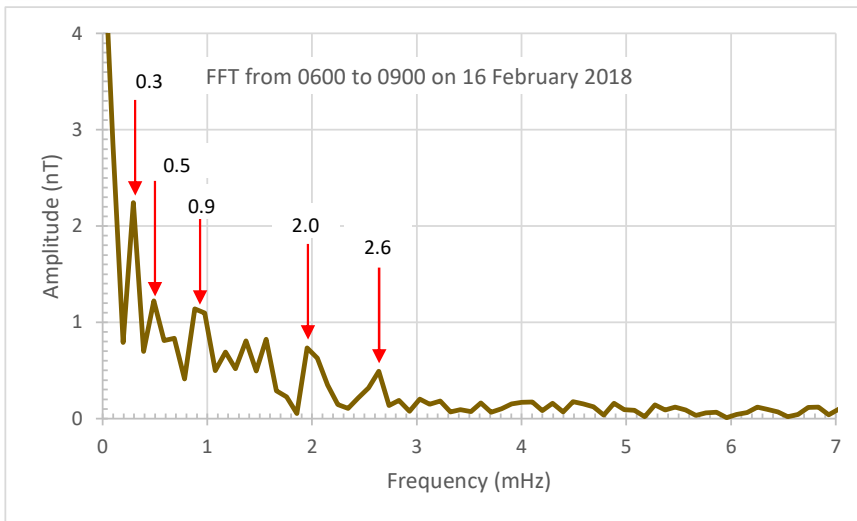


Figure 30.e ~ FFT of data from 0600 to 0900 on 16 February 2018 using 1024 datapoints. Although several frequencies are annotated, the signal amplitudes are low and probably noise except, possibly, one at 0.3 mHz (3333 s period).

2019 ▶

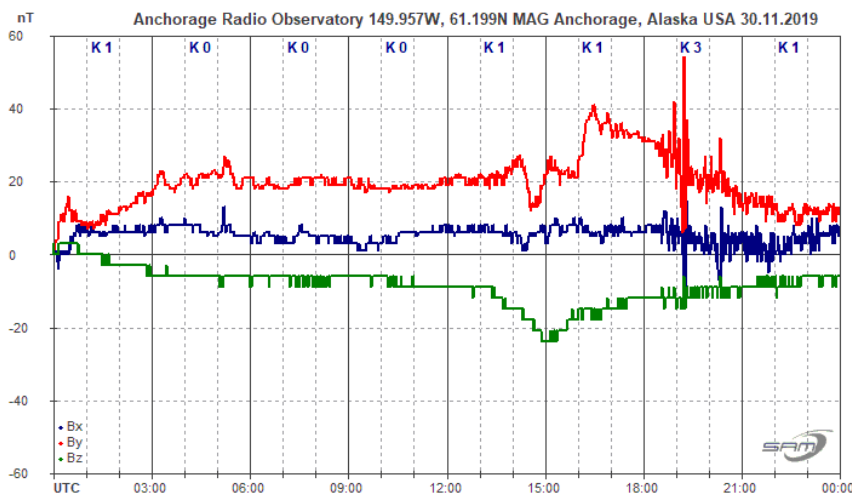
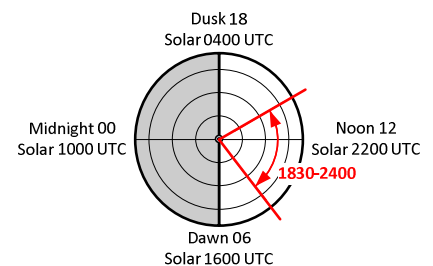


Figure 31 ~ ULF Waves start at 1830 on 30 November and continue until about 0400 the next day; see next figure.



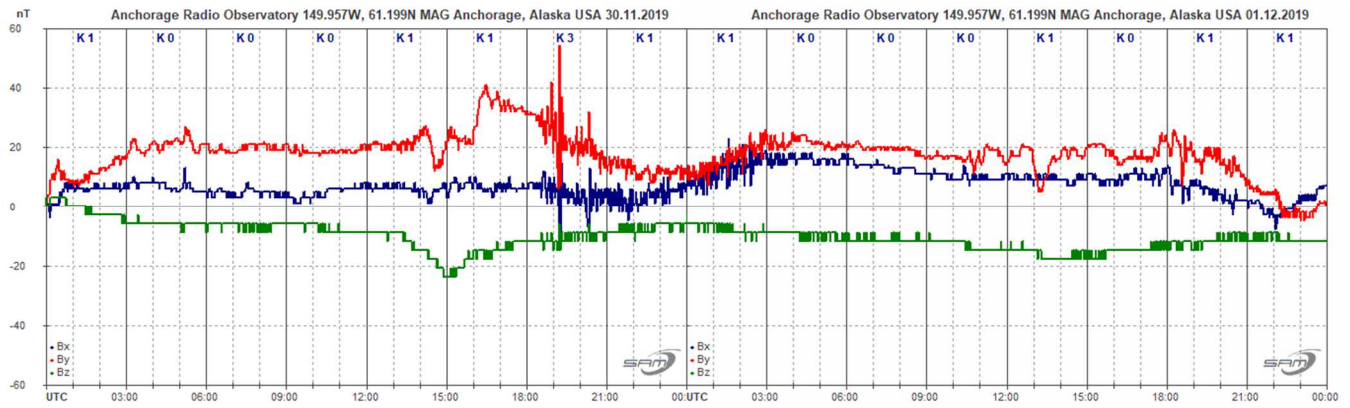
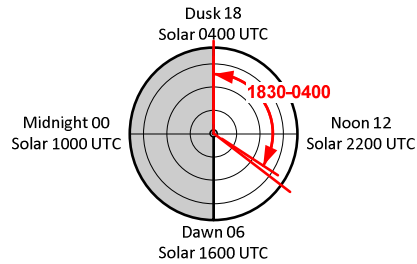


Figure 32 ~ Two 24 hour magnetograms have been spliced together to show ULF Waves that span UTC midnight on 30 November and 1 December 2019. They continue for almost 10 hours from 1830 on 30 November to 0400 on 1 December.



2020 ▶

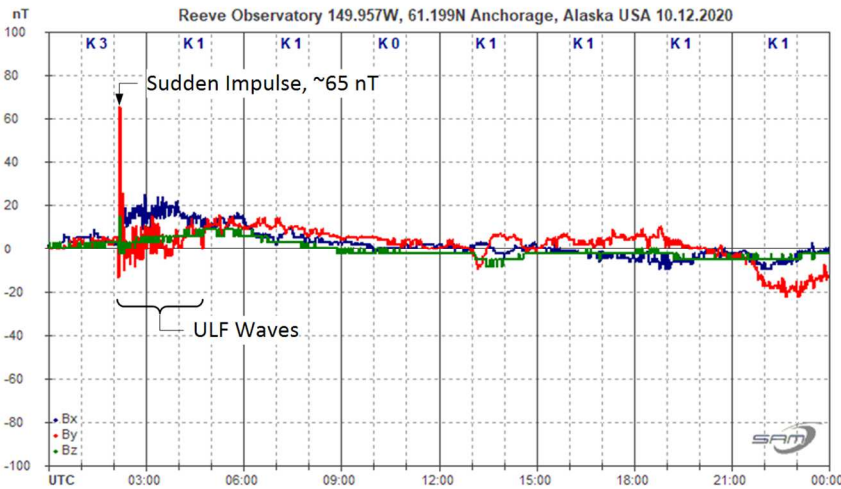
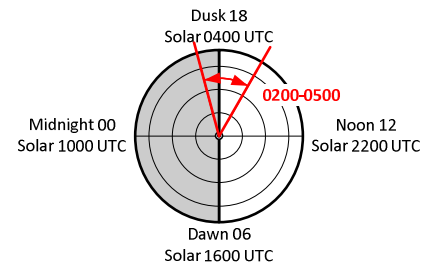


Figure 33 ~ ULF Waves start immediately after a sudden impulse at approximately 0215 and last a few hours on 10 December 2020.



2021 ▶

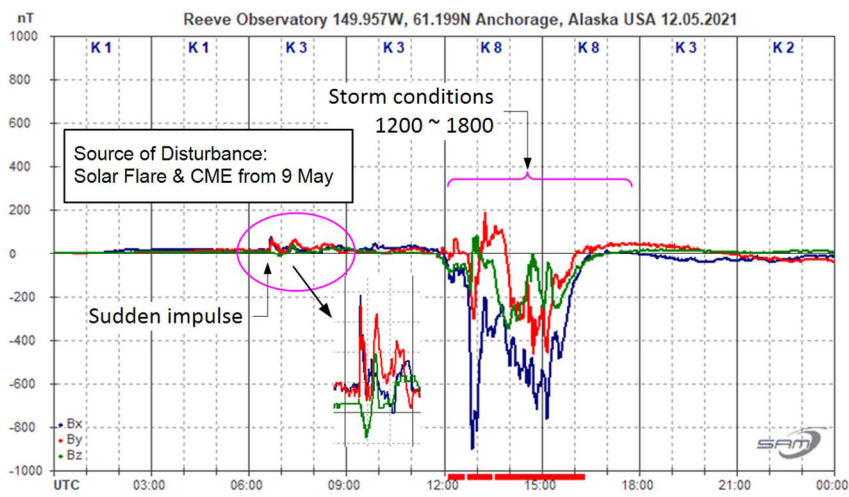


Figure 34 ~ The large deflections likely hide ULF Waves but strong periodic structures modulate the magnetic bay starting at 1200 on 12 May 2021.

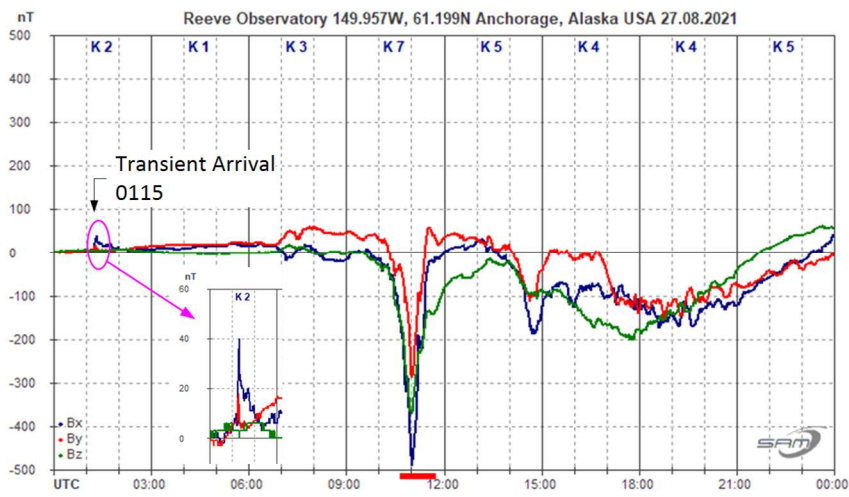
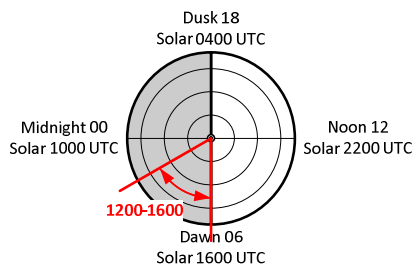
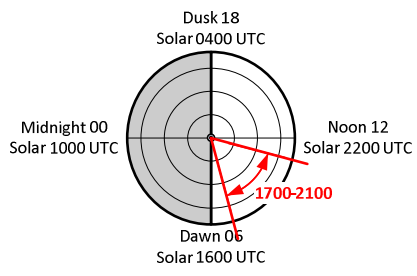


Figure 35 ~ A magnetic transient at 0115 eventually led to a geomagnetic storm during the 0900-1200 and 1200-1500 synoptic periods on 27 August 2021. ULF Waves are observed between about 1700 and 2100.



2022 ▶

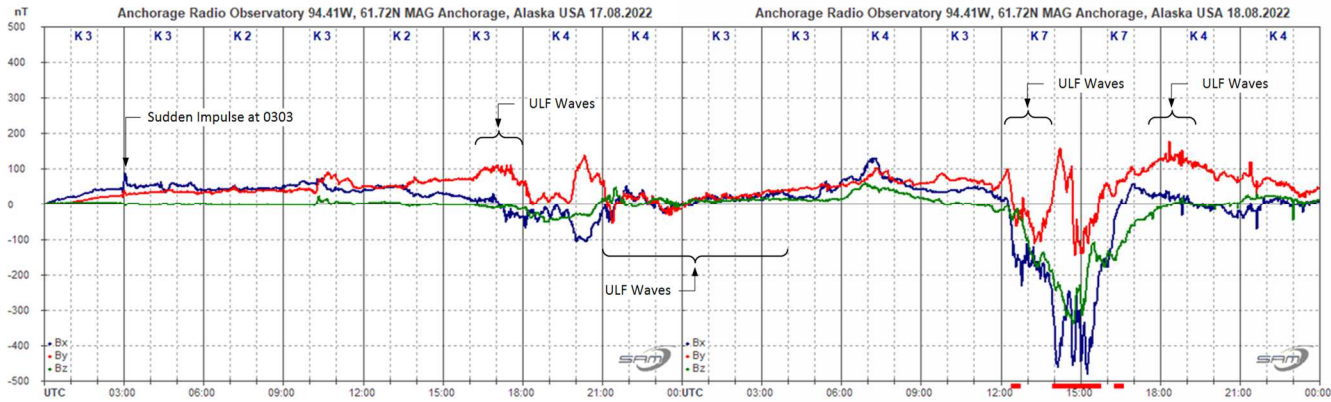


Figure 36.a ~ Two 24 hour magnetograms spliced together ~ to show the sequence of events after a sudden impulse at 0303 UTC on 17 August 2022. The sudden impulse resulted from a coronal mass ejection a few days before. There were relatively mild follow-on geomagnetic disturbances about 14 hours later at 1700 through 2300. ULF Waves also were

generated about the same time and appear between 1600 and 1800 and between 2100 and 2400 on 17 August, continuing until about 0400 the next day. Storm conditions were reached on 18 August during the 1200-1500 and 1500-1800 synoptic periods during which ULF waves also were observed.

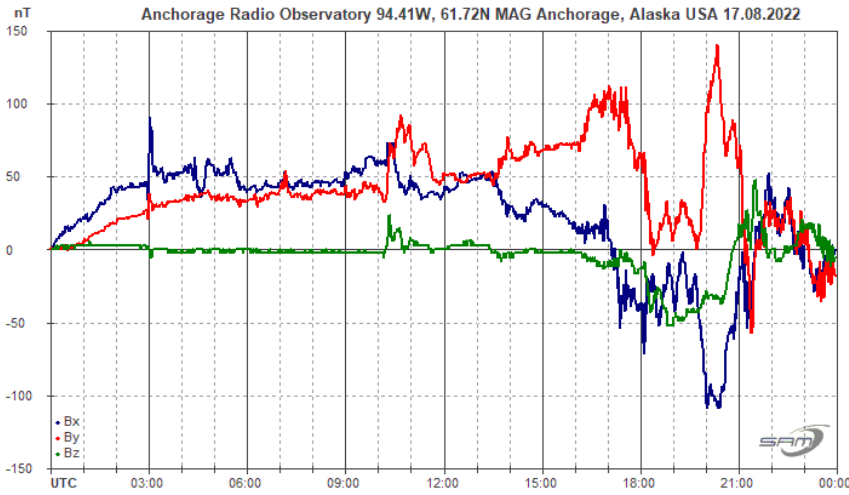


Figure 36.b ~ Magnetogram for 17 August more clearly shows the sudden impulse at 0303 and ULF Waves between approximately 1630 and 1800 and between 2100 and 2400, the latter spilling into the next day as shown below.

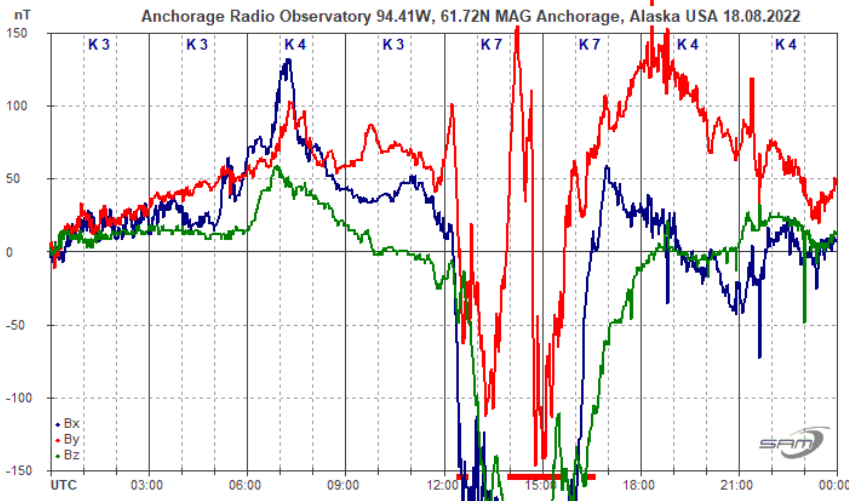
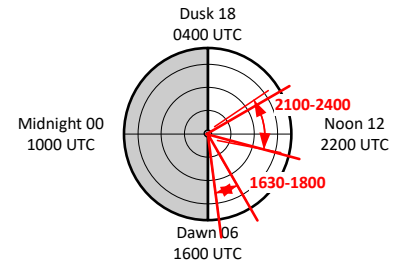


Figure 36.c ~ Magnetogram for 18 August at a fixed scale to show ULF Waves at the beginning of the UTC day from 0000 to about 0500. ULF Waves also are visible between approximately 1700 and 2400 in both the X- and Y-axes.

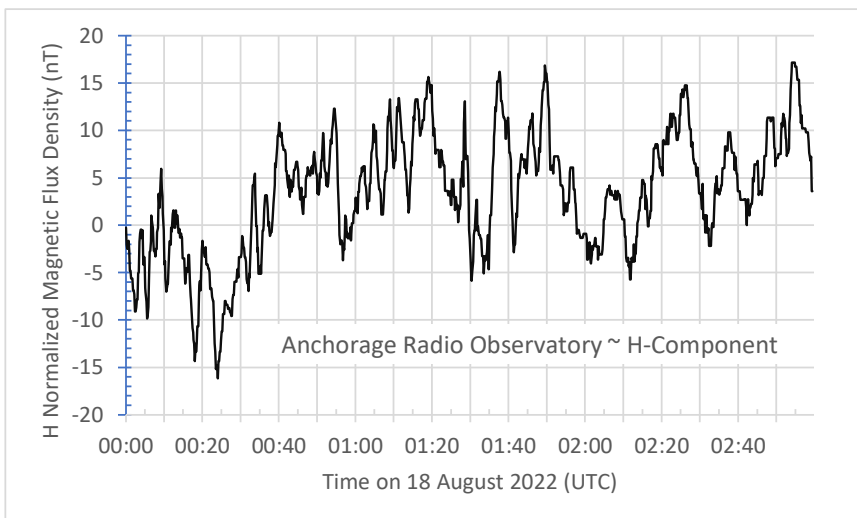


Figure 36.d ~ Normalized plot showing ULF Waves from 0000 to 0300 on 18 August. This plot shows the horizontal, or H, component, which is the vector sum of the X- and Y-axis magnetic flux density from the previous magnetogram. There are 51 cycles in this 3 hour time span, giving an average period of 212 s and an equivalent frequency of 4.7 mHz, very close to one of the so-called magic frequencies discussed in section 3.

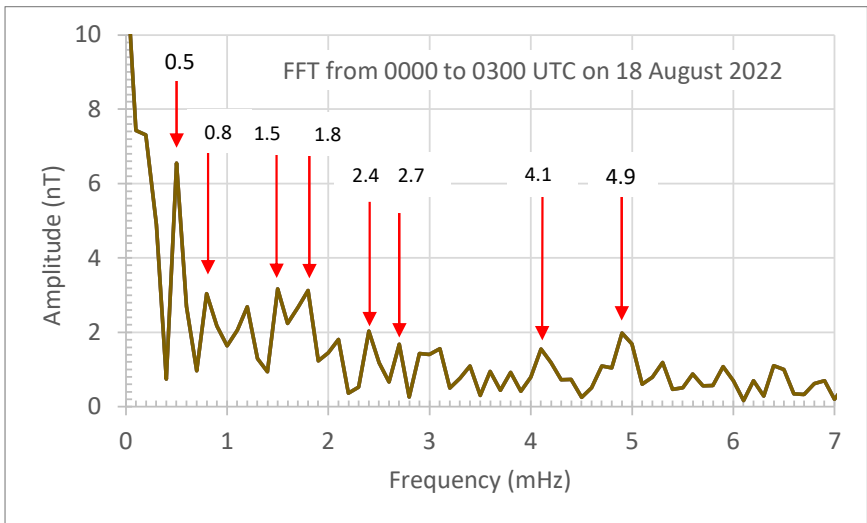
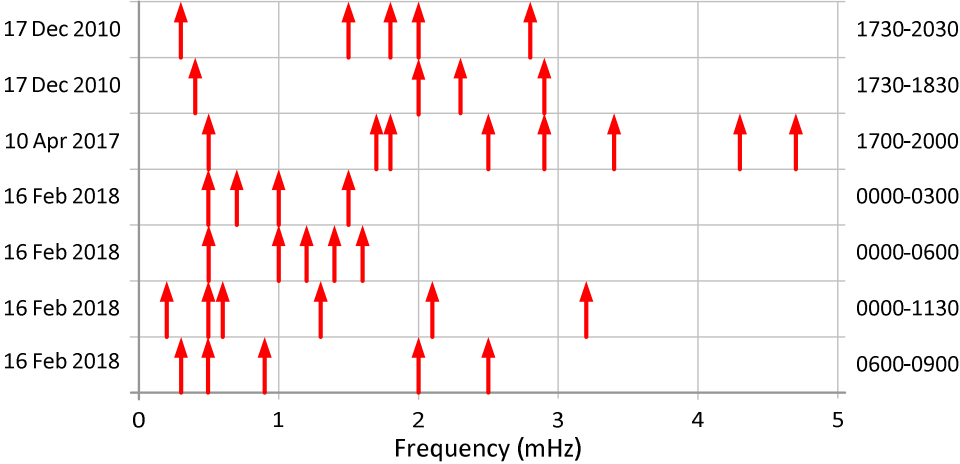


Figure 36.e ~ FFT analysis of 1024 datapoints for the time period 0000 to 0300 UTC on 18 August 2022. Annotated signals with amplitude less than 2 nT likely are noise, although the indication at 4.9 mHz appears to correlate with the manual counting method in the previous figure.

**II-2. Discussion**

A. All events analyzed using the FFT analysis were Pc5 and had frequencies < 5 mHz. All had frequency components outside the Pc5 range (< 1.7 mHz). The frequencies are summarized in figure 37 below. There are some apparent groupings but the number of events analyzed were too few to draw hard conclusions.

Figure 37 ~ Summary of events analyzed with Excel FFT Analysis tool



B. Most of the individual ULF Wave episodes analyzed in the previous section have frequencies within the Pc 5 frequency range. There may be several reasons: 1) Not all ULF Waves during the more than 10 year period in question were analyzed, and some unanalyzed waves may contain the higher frequencies of Pc 3 and Pc 4; 2) The relatively low sampling rate (100 mHz) of the magnetometer limits observations of the higher frequencies; or 3) The location of the Anchorage Radio Observatory (latitude, ground conductivity) is more conducive to the lower frequencies.

- C. Only a few Irregular Pulsations, Pi 1 or Pi 2, were specifically noted during the study period.
- D. ULF Waves were seldom seen during the solar midnight sector but were occasionally seen in the midnight-dawn sector.
- E. Longer period irregular oscillations, with periods of approximately 30 minutes to a few hours, are seen quite often in the Anchorage magnetograms. These last a few cycles and are not ULF Waves by definition. However, they could be related to longer Periodic Density Structures in the solar wind observed by NASA spacecraft [Reeve22B], or to periodic variations in the auroral electrojet due to geomagnetic substorms or resonance effects from subharmonics in the geomagnetic cavity. See, for example, the observations data for 14 June 2016, 15 September 2016, 17 October 2016 and 19 Jan 2018.
- F. Some episodes of ULF Waves recur several days in a row; for example, see observations data for 14-17 November 2020. It is not known if these are related to a single agent in the solar wind or multiple but unrelated dynamic pressure pulses that setup the conditions for ULF Waves over time.
- G. Many of the ULF Waves shown in the previous section occurred in the noon sector (solar noon  $\pm 3$  h), which implies they may be magnetosphere cavity oscillations or magnetic field line resonances in the dayside magnetosphere. ULF Waves in the dawn or dusk sectors, which were occasionally seen in the data, imply Kelvin-Helmholtz Waves caused by shear in the hydromagnetic interfaces between the solar wind and magnetopause.

### II-3. References & Weblinks

#### References:

- [Engebretson] Engebretson, M., Takahashi, K., Scholer, M., editors, Solar Wind Sources of Magnetospheric Ultra-Low-Frequency Waves, Geophysical Monograph 81, American Geophysical Union, 1994
- [Hughes] Hughes, W., Magnetospheric ULF Waves: A Tutorial with a Historical Perspective, Center for Space Physics, Boston University, 1994
- [Jacobs] Jacobs, J., Kato, Y., Matsushita, S., Troitskaya, V., Classifications of Geomagnetic Micropulsations, Journal of Geophysical Review, Vol. 69, No. 1, January 1, 1964
- [Mandea] Mandea, M., Korte, M., Yau, A., and Petrovsky, E., editors, Geomagnetism, Aeronomy and Space Weather: A Journey from the Earth's Core to the Sun, Special Publication of the International Union of Geodesy and Geophysics (IUGG), Cambridge University Press, 2020
- [McPherron] McPherron, R., Magnetic Pulsations: Their Sources and Relation to Solar Wind and Geomagnetic Activity, Surveys in Geophysics (2005), Springer, 2005, DOI 10.1007/s10712-005-1758-7
- [Rea] Rae, I., Watt, C., Fenrich, F., Mann, I., Ozeke, L., and Kale, A., Energy deposition in the ionosphere through a global field line resonance, Annals of Geophysics, No. 25, 2529–2539, 2007
- [Reeve21] Personal communications, Michael Hartinger (SCI), 26 August 2021

- [Reeve22B] Personal communications, Nickoleen Viall-Kepeco (NASA), 18 October 2022
- [Southwood] Southwood, D. and Hughes, W., Theory of Hydromagnetic Waves in the Magnetosphere, Space Science Reviews, Vol. 35 (1983), pg 301-366, D. Reidel Publishing Co. Boston, USA
- [Yumoto] Yumoto, K., Isono, A., Shiokawa, K., Matsuoka, H., Tanaka, Y., Menk, F., Fraser, B., Global Cavity Mode-Like and Localized Field-Line Pc 3-4 Oscillations Stimulated by Interplanetary Impulses (Si/Sc): Initial Results for the 210° MM Magnetic Observations, Solar Wind Sources of Magnetospheric Ultra-Low Frequency Waves, Geophysical Monograph 81, 1994
- [Zong] Zong, Q., Magnetospheric Response to Solar Wind Forcing: Ultra-Low Frequency Wave-Particle Interaction Perspective, Annales Geophysicae, Vol. 40, 121-150, 2022

Weblinks:

- {ESA} Earth's Bow Shock and Magnetosphere: [https://www.esa.int/ESA\\_Multimedia/Images/2015/01/Earth\\_s\\_bow\\_shock\\_and\\_magnetosphere](https://www.esa.int/ESA_Multimedia/Images/2015/01/Earth_s_bow_shock_and_magnetosphere)
- {NASA} Van Allen Radiation Belts: <https://www.nasa.gov/press/2014/august/nasa-probes-studying-earth-s-radiation-belts-to-celebrate-two-year-anniversary/>
- [Reeve22A] Reeve, W., HF Aurora Reflections Observed at Anchorage, Alaska USA, 2022, available at: [https://reeve.com/Documents/Articles%20Papers/Reeve\\_AuroraRadioObsrv.pdf](https://reeve.com/Documents/Articles%20Papers/Reeve_AuroraRadioObsrv.pdf)
- [SWPC] Solar Cycle Progression: <https://www.swpc.noaa.gov/products/solar-cycle-progression>
- {UAFGI} Auroral oval: <https://www.gi.alaska.edu/monitors/aurora-forecast>
-

## **Document Information**

Author: Whitham D. Reeve

Copyright: © 2023 W. Reeve

Revisions: 0.0 (Original draft started, 13 Apr 2022)

0.1 (Edited introduction and added sections, 23 Aug 2022)

0.2 (Added some observations, 24 Aug 2022)

0.3 (Started description of ULF Waves, 29 Aug 2022)

0.4 (Minor edits, 3 Sep 2022)

0.5 (Updated periodic density structures and magic frequencies, 17 Oct 2022)

0.6 (Edits to ULF Waves section, 07 Nov 2022)

0.7 (Continuing updates and FFT additions, 24 Nov 2022)

0.8 (Distribution, 25 Feb 2023)

0.9 (Presentation of paper SARA 2023 Western Conference, 17 Mar 2023)

Word count: 7986

File size (bytes): 7617718